



### Science Arts & Métiers (SAM)

is an open access repository that collects the work of Arts et Métiers Institute of Technology researchers and makes it freely available over the web where possible.

This is an author-deposited version published in: <https://sam.ensam.eu>  
Handle ID: <http://hdl.handle.net/10985/23274>



This document is available under CC BY-ND license

#### To cite this version :

Ramzi OTHMAN, Amine AMMAR, Khalid H. ALMITANI - Reduced modelling computation of layered soil's harmonic green functions - Finite Elements in Analysis and Design - Vol. 177, p.103419 - 2020

Any correspondence concerning this service should be sent to the repository

Administrator : [scienceouverte@ensam.eu](mailto:scienceouverte@ensam.eu)



# Reduced modeling Computation of layered soil's harmonic Green functions

Ramzi Othman<sup>1</sup>, Amine Ammar<sup>2</sup>, Khalid H. Almitani<sup>1</sup>

<sup>1</sup>Mechanical Engineering Department, Faculty of Engineering  
King Abdulaziz University, P.O. Box 80248,  
Jeddah 21589, Saudi Arabia

<sup>2</sup>LAMPA, Arts et Métiers ParisTech Angers, 2 Bd du Ronceray,  
49035 Angers, France

April 8, 2020

## Abstract

Ground-borne vibrations are disturbing to human beings. In order to model and reduce these vibrations, the calculation of the harmonic Green's-functions of the soil is highly required since the most effective numerical solution to predict ground-borne vibration is to couple the finite-element and the boundary-element methods. In this work, we elaborate a direct space-frequency formulation that is especially suitable of material exhibiting visco-elastic behavior. Moreover, an original formulation of the Proper Generalized Decomposition (PGD) reduction technique was undertaken in the frequency-space domain. This new approach highly shortens time computing costs. It is mainly valuable when a parametric study is concerned. Moreover, the PGD resolution allows providing an off-line solution, thus, the solution is calculated only once.

## Keywords

Ground-borne vibration; Layered viscoelastic soil; Proper Generalized Decomposition (PGD); Model reduction technique; Parametric analysis; Finite-element; Boundary-element; Railway traffic; Earthquakes.

# 1 Introduction

Railway traffic causes vibrations which are mainly due to the uneven nature of railway tracks, misalignment of wheels of the trains or discontinuities of the wheels and tracks [1]. For similar reasons, vibrations are also generated by other terrestrial vehicles traffics. Earthquakes can also initiate vibrations. These vibrations propagate through the soil to the foundations of neighboring buildings and structures, causing disturbances, noise pollution and sometimes damage [2, 3]. Moreover, they can also have unwelcome effects on the health of occupants and they can disturb the work of vibration-sensitive equipment. To prevent these undesirable effects, ground-borne vibrations have to be reduced or isolated as much as possible.

The formulation of a suitable model is difficult because of the number of parameters involved in describing the underground environment. For modelling of vibrations due to the underground train traffic, the tunnel structure and the surrounding soil are assumed much stiffer than the track [4]. Due to this assumption, the railway induced vibrations problem is approached in two steps. Firstly, the wheel-rail-(track) interaction problem is separately solved to derive the dynamic axle forces. These forces are considered as an input external force for the second problem that deals with the track-(tunnel)-soil interaction problem. These problems aim at predicting the vibration propagation in the underground environment.

Various models are designed to predict railway traffic-induced vibration [5]. The numerical solutions obtained earlier were time-consuming because of the slow processing speeds of computers. Analytical approaches were preferred. However, with the help of increasing processing speeds of computers, the calculation time can be reduced admirably. Now, numerical models are highly preferred in the modelling of underground railway-induced vibrations, mainly by using finite/infinite-element models [6] and coupled finite element–boundary element (FE–BE) models [7, 8].

Even though two-dimensional numerical models offer computation times that are much shorter than three-dimensional models [9], they are unable to account for wave propagation along the track. In addition, they cannot accurately simulate the radiation damping of the soil [7]. On the other hand, 3-D numerical models are highly expensive in terms of computation requirements. In addition to theoretical approaches [10, 11, 12, 13, 14], numerical methods that exploit the invariance in structure (track and tunnel) longitudinal axis direction (2.5D finite/infinite element or FE–BE models) are attracting a particular attention from the scientific community [15, 16, 17, 18, 19, 20]. These techniques are effective when considering very long structures partially or totally embedded in soil [9, 21]. They indeed take into account the soil-structure coupling which is of great importance [22, 23]. The structure is modeled by techniques of structural dynamics that can be deterministic or probabilistic [24]. The soil is regarded

as a layered half-space, which is made of horizontal elastic homogenous layers that rest on a homogenous elastic half-space. The Green's-function [25] or the fundamental solutions [26] can be used to describe the dynamic characteristics of a layered half-space.

The fundamental solutions are based on the computation of integrals that require the introduction of a fictitious boundary, across which the radiation conditions have to be satisfied [27]. The Green's functions are approached in two different ways: approximate and analytical solutions. An example of approximate methods is the thin-layer method [28]. The analytical methods give solutions that are expressed in terms of integrals that have infinite or semi-infinite integration paths [29, 30, 31, 32]. Franssens [33] used the propagator matrix method to calculate the inverse Fourier integrands. Cairo et al. [34] and Kausel [35] used the Stiffness Matrix Method. Zhang et al. [36] used wavenumber integration method. Shaukath et al. [37] computed Green functions using an axisymmetric finite element approach and a time-explicit integration.

In this work, we make a direct space-frequency formulation that is especially suitable of material exhibiting visco-elastic behavior. The advantage of this formulation is that it allows finding the real and complex part of the displacement field and thus permitting to find the frequency response without making any explicit or implicit time integration. Moreover, the Proper-Generalized-Decomposition (PGD) reduction method [38, 39, 40, 41, 42] is used to drastically reduce the computation time. **It is** a very powerful technique to deal with large-sized numerical models in a wide range of engineering fields [43, 44, 45]. *However, the PGD method has rarely been used in the space-frequency domain.* In the papers [46] and [47] the dynamic problem is solved with technique which combines the Variational Theory of Complex Rays (VTCR) with Proper Generalized Decomposition (PGD) and does not require the resolution of acoustic problems at many frequencies. The PGD is used to find a representation of the approximate solution which is separated between two variables, the wave propagation direction and the frequency. However this works uses the pressure as a primary variable and does not uses a tensoriel separation of the global operator (which can come back a bit expensive in terms of allocated memory). A formulation of the PGD method in frequency domain was also presented in [49], [50] and [48]. **The PGD method is then used to compute space-frequency separated representations by considering the frequency as an extra coordinate [49, 48].** Our work is distinguished by:

- The use of the viscoelastic constitutive behaviour to introduce naturally the damping. - Consequently the kinematic field (displacement) is naturally formulated with the complex components involving a system which is twice larger than the usually solved in harmonic resolution.
- The operators of our PGD decomposition (with parametrization or using frequency as an extra coordinate) are written in terms of tensor decomposition alleviating the cost of the reformulation of the PGD for each case of decomposition.

## 2 Problem statement

In this work, we aim at computing the Green functions of a layered soil, while scaling down the computation time using a model reduction technique. These functions are the displacement response of the layered soil caused by a concentrated force of unit magnitude (Figure 1(a)). The geometry of the problem is

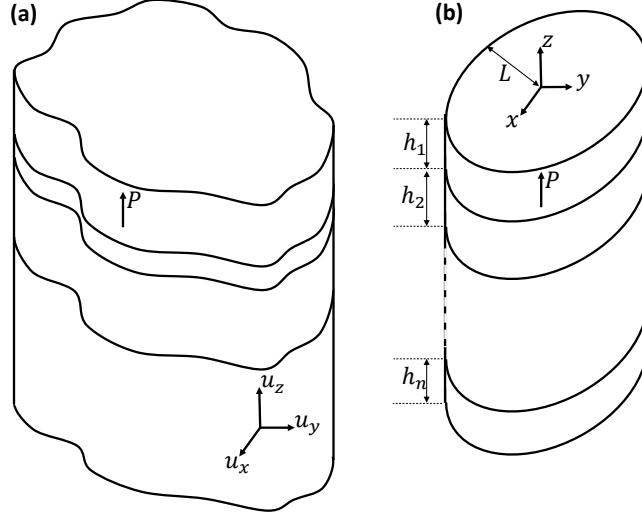


Figure 1: Layered soil: (a) unbounded geometry, and (b) bounded geometry

a general 3D. We denote by  $\mathbf{x} = (x, y, z)$  the position vector. Without loss of generality, the soil domain can be defined as  $\{\mathbf{x} \in \mathbb{R}^3; z \leq 0\}$ . Consequently, the soil domain is infinite in the  $x$  and  $y$  directions and semi-infinite in the  $z$  direction. However, the unbounded domain is unsuitable for finite element analysis. Thus, it is imperative to introduce virtual boundaries on the three directions. In this work, the bounded soil is defined by (Figure 1(b)):

$$\Omega = \left\{ \mathbf{x} \in \mathbb{R}^3; 0 \leq r \leq L, r = \sqrt{(x^2 + y^2)}, -\sum_{j=1}^n h_j \leq z \leq 0 \right\}, \quad (1)$$

where  $L$  denotes the horizontal distance that separates the concentrated load to the virtual vertical boundary,  $n$  is the considered number of layers, and  $h_j$  is the height of  $j^{th}$  ( $1 \leq j \leq n$ ) layer which is defined by:

$$\Omega_j = \left\{ \mathbf{x} \in \Omega; -\sum_{k=1}^j h_k \leq z \leq -\sum_{k=1}^{j-1} h_k \right\}. \quad (2)$$

$L$  defines a range of investigation. Indeed, the displacement induced by the concentrated load drastically vanishes as the distance from the load increases. The range of influence of the load is limited to some region around it. However, the virtual boundaries can induce some numerical discrepancies as they create some non-physical and purely numerical wave reflections. On one hand,  $L$  should be increased to delay the effects of the boundary-induced wave reflections. On the hand,  $L$  should be reduced to decrease the size of the numerical model and the computation time. Using a reduction model technique is a main advantage here as it permits to enlarge  $L$  and the size of the numerical model, thus, solving the tradeoff between reducing computation time and reducing the effects of wave reflections occurring at virtual boundaries.

The discussion presented above for  $L$  is also true for  $n$  and  $h_n$ . Indeed, to make the vertical dimension of the layered soil bound, it is necessary to limit the number of layers to a bounded number  $n$  and/or to bound the height of the deepest layer.

We are interested in calculating the displacement field  $\mathbf{u}(\mathbf{x}, t) = \mathbf{u}(x, y, z, t)$ , over the domain  $\Omega$ , due to a unit concentrated harmonic force. Without any loss of generality, this load can be applied in  $\mathbf{x}_0 = (x_0 = 0, y_0 = 0, z_0)$ . This makes that the horizontal dimension is centered around the load position. In Figure 1, the load is depicted along the vertical direction, but it can also take any of the two horizontal directions. Considering symmetry, quarter of the bounded geometry is modeled (Figure 2) in the case of a vertical force. However, in the case of horizontal force, half of the bounded geometry is modeled (Figure 3).

The interface between the  $j^{th}$  and  $(j+1)^{th}$  layers is defined as:  $\Gamma_j^z = \{\mathbf{x} \in \Omega; z = -\sum_{k=1}^j h_k\}$ . We also define the following surfaces:

- $\Gamma_0^z = \{\mathbf{x} \in \Omega; z = 0\}$  : the upper surface denoted by (5) in Figure 2,
- $\Gamma_n^z = \{\mathbf{x} \in \Omega; z = -\sum_{k=1}^n h_k\}$  : the bottom surface denoted by (4) in Figure 2,
- $\Gamma^x = \{\mathbf{x} \in \Omega; x = 0\}$  : the surface (3) on Figure 2,
- $\Gamma^y = \{\mathbf{x} \in \Omega; y = 0\}$  : the surface (1) on Figure 2, and
- $\Gamma^r = \{\mathbf{x} \in \Omega; r = L, r = \sqrt{(x^2 + y^2)}\}$  : the surface (2) on Figure 2.

In the case of a model involving half of the geometry, i.e., in the case of horizontal forces, we are not dealing with surface (3).

The problem is governed by the set of the following equations

$$\rho(\mathbf{x}) \frac{\partial^2 \mathbf{u}}{\partial t^2} - \nabla \cdot \boldsymbol{\sigma} - \mathbf{f} = 0, \quad (3)$$

$$\boldsymbol{\sigma} = \lambda \text{tr}(\boldsymbol{\varepsilon}) \mathbf{1} + 2\mu \boldsymbol{\varepsilon}, \text{ and} \quad (4)$$

$$\boldsymbol{\sigma} = \frac{\nabla \mathbf{u} + \nabla^T \mathbf{u}}{2}, \quad (5)$$

defining the momentum equilibrium, the constitutive law and the small strain definition, respectively. In the above equations  $\rho$  is the density,  $\boldsymbol{\sigma}$  is the stress tensor,  $\boldsymbol{\varepsilon}$  is the strain tensor,  $\lambda$ ,  $\mu$  are the Lamé coefficients,  $\mathbf{f}$  represents the body forces and  $\mathbf{1}$  is the identity tensor.

The boundary conditions are given by:

- A concentrated harmonic force along the vertical direction  $F_z(\mathbf{x}_0) = F_0 \exp(i\omega t)$
- Symmetric conditions imposed to the displacement field on the boundaries  $\Gamma^x$  and  $\Gamma^y$
- Damping conditions on  $\partial\Omega_{damp} = \Gamma_n^z \cup \Gamma^r$  that writes  $\boldsymbol{\sigma} \cdot \mathbf{n} = \eta \dot{\mathbf{u}}$  where  $\mathbf{n}$  is the outward unit normal vector to the surface. This is mainly introduced to reduce wave reflections from the virtual boundaries  $\Gamma_n^z$  and  $\Gamma^r$  that are introduced here to limit the unbounded geometry of the layered soil.
- Between the layers we assume continuity of the displacement field and of the normal stress vector.

### 3 Problem formulation

The equation to be solved is:

$$\rho(\mathbf{x}) \frac{\partial^2 \mathbf{u}}{\partial t^2} - \nabla \cdot \boldsymbol{\sigma} - \mathbf{f} = 0. \quad (6)$$

In the absence of volume forces, the variational formulation on  $\Omega$  writes

$$\int_{\Omega} \left( \rho(\mathbf{x}) V^* \frac{\partial^2 \mathbf{u}}{\partial t^2} - V^* (\nabla \cdot \boldsymbol{\sigma}) \right) d\Omega = 0. \quad (7)$$

An integration by part is undertaken. With this integration the domain boundary is decomposed onto two parts: (i) the node on which the concentrated force is applied and (ii) the boundary containing damping conditions. Then we obtain

$$\int_{\Omega} \rho(\mathbf{x}) V^* \frac{\partial^2 \mathbf{u}}{\partial t^2} d\Omega + \int_{\Omega} \boldsymbol{\varepsilon}^* : \boldsymbol{\sigma} d\Omega - \int_{\partial\Omega_{damp}} V^* (\boldsymbol{\sigma} \cdot \mathbf{n}) d(\partial\Omega) = V_f^* F(t), \quad (8)$$

where  $\mathbf{n}$  is the outward normal vector to the damping surface,  $V_f^*$  corresponds to the virtual degree of freedom of the node on which the concentrated force is applied and  $\partial\Omega_{damp} = \Gamma_n^z \cup \Gamma^r$  is the part of the boundary on which we can write that

$$\boldsymbol{\sigma} \cdot \mathbf{n} = \eta \frac{\partial \mathbf{u}}{\partial t}. \quad (9)$$

Thus, the surface integral of Eq. (8) becomes

$$\int_{\partial\Omega_{damp}} V^* \cdot (\boldsymbol{\sigma} \cdot \mathbf{n}) d(\partial\Omega) = \int_{\partial\Omega_{damp}} \eta V^* \cdot \frac{\partial \mathbf{u}}{\partial t} d(\partial\Omega). \quad (10)$$

For the sake of clarity while constructing the operators, and without loss of generality, we are going to illustrate the 2D case in the coming equations. The 3D extension will not be fundamentally different. The notations of the kinematic field derivatives will be  $\frac{\partial \mathbf{u}}{\partial t} = \dot{\mathbf{u}}$  and  $\frac{\partial^2 \mathbf{u}}{\partial t^2} = \ddot{\mathbf{u}}$ . Moreover, in vectorial notation the stress and strain tensors are given by:

$$\boldsymbol{\sigma} = \begin{pmatrix} \sigma_{xx} \\ \sigma_{yy} \\ \sigma_{xy} \end{pmatrix} \quad (11)$$

and

$$\boldsymbol{\varepsilon} = \begin{pmatrix} \varepsilon_{xx} \\ \varepsilon_{yy} \\ 2\varepsilon_{xy} \end{pmatrix}. \quad (12)$$

Eq. (8) is then rewritten as follows:

$$\int_{\Omega} \rho(\mathbf{x}) V^* \ddot{\mathbf{u}} d\Omega + \int_{\Omega} \boldsymbol{\varepsilon}^{*T} \cdot \boldsymbol{\sigma} d\Omega - \int_{\partial\Omega_{damp}} \eta V^* \cdot \dot{\mathbf{u}} d(\partial\Omega) = V_f^* F(t). \quad (13)$$

Now we are going to write the constitutive equation. Each soil layer is assumed visco-elastic. Consequently, the stress-strain relation is written:

$$\boldsymbol{\sigma} = \lambda(\mathbf{x}, \omega) \text{tr}(\boldsymbol{\varepsilon}) \mathbf{1} + 2\mu(\mathbf{x}, \omega) \boldsymbol{\varepsilon}, \quad (14)$$

where the Lamé constants  $\lambda(\mathbf{x}, \omega)$  and  $\mu(\mathbf{x}, \omega)$  are depending on the vector position  $\mathbf{x}$  to account for the different layers of the soil; they are also depending on the solicitation frequency to account for the visco-elastic behavior of each layer. Using a fourth order tensor  $C(\mathbf{x}, \omega)$ , the constitutive law of Eq. (14) writes:

$$\begin{pmatrix} \sigma_{xx} \\ \sigma_{yy} \\ \sigma_{xy} \end{pmatrix} = C(\mathbf{x}, \omega) \begin{pmatrix} \varepsilon_{xx} \\ \varepsilon_{yy} \\ 2\varepsilon_{xy} \end{pmatrix}. \quad (15)$$

$C(\mathbf{x}, \omega)$  accounts for the visco-elastic behavior of each soil layer. As illustration, this fourth order tensor is expressed in the case of plane strain as:

$$C(\mathbf{x}, \omega) = \begin{pmatrix} \lambda(\mathbf{x}, \omega) + 2\mu(\mathbf{x}, \omega) & \lambda(\mathbf{x}, \omega) & 0 \\ \lambda(\mathbf{x}, \omega) & \lambda(\mathbf{x}, \omega) + 2\mu(\mathbf{x}, \omega) & 0 \\ 0 & 0 & \mu(\mathbf{x}, \omega) \end{pmatrix}. \quad (16)$$

In order to establish the frequency-space discrete formulation, we need to separate the contribution of the two Lamé coefficients

$$\begin{pmatrix} \sigma_{xx} \\ \sigma_{yy} \\ \sigma_{xy} \end{pmatrix} = \lambda(\mathbf{x}, \omega) \begin{pmatrix} 1 & 1 & 0 \\ 1 & 1 & 0 \\ 0 & 0 & 0 \end{pmatrix} \begin{pmatrix} \varepsilon_{xx} \\ \varepsilon_{yy} \\ 2\varepsilon_{xy} \end{pmatrix} + \mu(\mathbf{x}, \omega) \begin{pmatrix} 2 & 0 & 0 \\ 0 & 2 & 0 \\ 0 & 0 & 1 \end{pmatrix} \begin{pmatrix} \varepsilon_{xx} \\ \varepsilon_{yy} \\ 2\varepsilon_{xy} \end{pmatrix}. \quad (17)$$

From the displacement field

$$\mathbf{u} = \begin{pmatrix} u_x \\ u_y \end{pmatrix}, \quad (18)$$

we can then express the strain and the virtual strain corresponding to the primary field and the test field as

$$\varepsilon = \begin{pmatrix} \frac{\partial}{\partial x} & 0 \\ 0 & \frac{\partial}{\partial y} \\ \frac{\partial}{\partial y} & \frac{\partial}{\partial x} \end{pmatrix} \begin{pmatrix} u_x \\ u_y \end{pmatrix}, \quad (19)$$

and

$$\varepsilon^* = \begin{pmatrix} u^* & v^* \end{pmatrix} \begin{pmatrix} \frac{\partial}{\partial x} & 0 & \frac{\partial}{\partial y} \\ 0 & \frac{\partial}{\partial y} & \frac{\partial}{\partial x} \end{pmatrix}, \quad (20)$$

respectively. Let  $\mathbf{N}(\mathbf{x})$  denotes the space interpolation from the discrete displacement field. The components of the continuum displacement field are given by

$$u_x = \mathbf{N}^T(\mathbf{x}) \cdot \mathbf{u}_x, \quad (21)$$

and

$$u_y = \mathbf{N}^T(\mathbf{x}) \cdot \mathbf{u}_y, \quad (22)$$

where  $\mathbf{u}_x$  and  $\mathbf{u}_y$  contains the nodal components of the kinematic field which depend here on frequency as we have formulated the elastodynamic problem in the frequency-space domain. Consequently, the strain writes:

$$\varepsilon = \begin{pmatrix} \frac{\partial}{\partial x} & 0 \\ 0 & \frac{\partial}{\partial y} \\ \frac{\partial}{\partial y} & \frac{\partial}{\partial x} \end{pmatrix} \cdot \begin{pmatrix} \mathbf{N}^T(\mathbf{x}) \cdot \mathbf{u}_x \\ \mathbf{N}^T(\mathbf{x}) \cdot \mathbf{u}_y \end{pmatrix} = \begin{pmatrix} \frac{\partial \mathbf{N}^T(\mathbf{x})}{\partial x} & 0 \\ 0 & \frac{\partial \mathbf{N}^T(\mathbf{x})}{\partial y} \\ \frac{\partial \mathbf{N}^T(\mathbf{x})}{\partial y} & \frac{\partial \mathbf{N}^T(\mathbf{x})}{\partial x} \end{pmatrix} \cdot \begin{pmatrix} \mathbf{u}_x \\ \mathbf{u}_y \end{pmatrix}. \quad (23)$$

Moreover, the test field can be written as:

$$\begin{pmatrix} u^* & v^* \end{pmatrix} = \begin{pmatrix} \mathbf{u}^{*T} & \mathbf{v}^{*T} \end{pmatrix} \begin{pmatrix} \mathbf{N}(\mathbf{x}) \\ \mathbf{N}(\mathbf{x}) \end{pmatrix}. \quad (24)$$

Thus, the virtual strain writes:

$$\varepsilon^* = \begin{pmatrix} \mathbf{u}^{*T} & \mathbf{v}^{*T} \end{pmatrix} \begin{pmatrix} \frac{\partial \mathbf{N}(\mathbf{x})}{\partial x} & 0 & \frac{\partial \mathbf{N}(\mathbf{x})}{\partial y} \\ 0 & \frac{\partial \mathbf{N}(\mathbf{x})}{\partial y} & \frac{\partial \mathbf{N}(\mathbf{x})}{\partial x} \end{pmatrix}. \quad (25)$$

For the sake of clarity, the notation  $\mathbf{N}(\mathbf{x})$  will simply be denoted  $\mathbf{N}$ . Accordingly, the visco-elastic deformation energy within the bounded soil domain is evaluated as follows:

$$\begin{aligned} \int_{\Omega} \varepsilon^{*T} \cdot \sigma d\Omega = & \int_{\Omega} \left( \mathbf{u}^{*T} \quad \mathbf{v}^{*T} \right) \begin{pmatrix} \frac{\partial \mathbf{N}}{\partial x} & 0 & \frac{\partial \mathbf{N}}{\partial y} \\ 0 & \frac{\partial \mathbf{N}}{\partial y} & \frac{\partial \mathbf{N}}{\partial x} \end{pmatrix} \left[ \lambda(\mathbf{x}, \omega) \begin{pmatrix} 1 & 1 & 0 \\ 1 & 1 & 0 \\ 0 & 0 & 0 \end{pmatrix} \right. \\ & \left. + \mu(\mathbf{x}, \omega) \begin{pmatrix} 2 & 0 & 0 \\ 0 & 2 & 0 \\ 0 & 0 & 1 \end{pmatrix} \right] \begin{pmatrix} \frac{\partial \mathbf{N}^T}{\partial x} & 0 \\ 0 & \frac{\partial \mathbf{N}^T}{\partial y} \\ \frac{\partial \mathbf{N}^T}{\partial y} & \frac{\partial \mathbf{N}^T}{\partial x} \end{pmatrix} \begin{pmatrix} \mathbf{u}_x \\ \mathbf{u}_y \end{pmatrix} d\Omega. \end{aligned} \quad (26)$$

After some simplifications:

$$\begin{aligned} \int_{\Omega} \varepsilon^{*T} \cdot \sigma d\Omega = & \left( \mathbf{u}^{*T} \quad \mathbf{v}^{*T} \right) \left[ \int_{\Omega} \lambda(\mathbf{x}, \omega) \begin{pmatrix} \frac{\partial \mathbf{N}}{\partial x} \frac{\partial \mathbf{N}^T}{\partial x} & \frac{\partial \mathbf{N}}{\partial x} \frac{\partial \mathbf{N}^T}{\partial y} \\ \frac{\partial \mathbf{N}}{\partial y} \frac{\partial \mathbf{N}^T}{\partial x} & \frac{\partial \mathbf{N}}{\partial y} \frac{\partial \mathbf{N}^T}{\partial y} \end{pmatrix} d\Omega \right. \\ & \left. + \int_{\Omega} \mu(\mathbf{x}, \omega) \begin{pmatrix} 2 \frac{\partial \mathbf{N}}{\partial x} \frac{\partial \mathbf{N}^T}{\partial x} + \frac{\partial \mathbf{N}}{\partial y} \frac{\partial \mathbf{N}^T}{\partial y} & \frac{\partial \mathbf{N}}{\partial y} \frac{\partial \mathbf{N}^T}{\partial x} \\ \frac{\partial \mathbf{N}}{\partial x} \frac{\partial \mathbf{N}^T}{\partial y} & 2 \frac{\partial \mathbf{N}}{\partial y} \frac{\partial \mathbf{N}^T}{\partial y} + \frac{\partial \mathbf{N}}{\partial x} \frac{\partial \mathbf{N}^T}{\partial x} \end{pmatrix} d\Omega \right] \begin{pmatrix} \mathbf{u}_x \\ \mathbf{u}_y \end{pmatrix}. \end{aligned} \quad (27)$$

At this stage, it is very important to define the expressions of Lamé coefficients. As we are going to study the case of harmonic excitation:

$$F(t) = F_0 \exp(i\omega t), \quad (28)$$

the Lamé coefficients are defined using complex number representation in order to take into account the visco-elastic properties of the soil. Namely,

$$\lambda(\mathbf{x}, \omega) = \sum_j p_j'(\mathbf{x}) q_j'(\omega) + i \sum_j p_j''(\mathbf{x}) q_j''(\omega) \quad (29)$$

$$\mu(\mathbf{x}, \omega) = \sum_j r_j'(\mathbf{x}) s_j'(\omega) + i \sum_j r_j''(\mathbf{x}) s_j''(\omega) \quad (30)$$

$j$  denotes the layer index. This type of definition allows: (i) to take into account different visco-elastic behaviors for the different layers, and (ii) to separate the space and frequency dependency, *which is very important later for PGD formulation*. Typically if the behavior is homogeneous within each layer the function  $p_j'(\mathbf{x})$  will depend only on the  $z$  direction and will be defined as a rectangular function that is equal to 1 on the layer that behavior is given by  $q_j'(\omega)$  and vanish (value = 0) on the other layers. Namely,

$$p_j'(\mathbf{x}) = \begin{cases} 1 & \text{if } -\sum_{k=1}^j h_k < z \leq -\sum_{k=1}^{j-1} h_k \\ 0 & \text{otherwise} \end{cases} \quad (31)$$

This general definition also allows to take into account the multimodal behavior of each layer. In that case, it is possible to write the function  $q_j'(\omega)$  as a sum of different function depending on the frequency  $\omega$ . The same advantages hold for the other terms  $p_j''(\mathbf{x}) q_j''(\omega)$ ,  $r_j'(\mathbf{x}) s_j'(\omega)$ , and  $r_j''(\mathbf{x}) s_j''(\omega)$ . Accordingly, it is possible to rewrite the terms of the last form of Eq. (27) of the variational formulation as:

$$\begin{aligned} & \int_{\Omega} \lambda(\mathbf{x}, \omega) \begin{pmatrix} \frac{\partial \mathbf{N}}{\partial x} \frac{\partial \mathbf{N}^T}{\partial x} & \frac{\partial \mathbf{N}}{\partial x} \frac{\partial \mathbf{N}^T}{\partial y} \\ \frac{\partial \mathbf{N}}{\partial y} \frac{\partial \mathbf{N}^T}{\partial x} & \frac{\partial \mathbf{N}}{\partial y} \frac{\partial \mathbf{N}^T}{\partial y} \end{pmatrix} d\Omega \\ &= \int_{\Omega} \left( \sum_j p_j'(\mathbf{x}) q_j'(\omega) + i \sum_j p_j''(\mathbf{x}) q_j''(\omega) \right) \begin{pmatrix} \frac{\partial \mathbf{N}}{\partial x} \frac{\partial \mathbf{N}^T}{\partial x} & \frac{\partial \mathbf{N}}{\partial x} \frac{\partial \mathbf{N}^T}{\partial y} \\ \frac{\partial \mathbf{N}}{\partial y} \frac{\partial \mathbf{N}^T}{\partial x} & \frac{\partial \mathbf{N}}{\partial y} \frac{\partial \mathbf{N}^T}{\partial y} \end{pmatrix} d\Omega \end{aligned} \quad (32)$$

This integral also writes:

$$\begin{aligned} & \int_{\Omega} \lambda(\mathbf{x}, \omega) \begin{pmatrix} \frac{\partial \mathbf{N}}{\partial x} \frac{\partial \mathbf{N}^T}{\partial x} & \frac{\partial \mathbf{N}}{\partial x} \frac{\partial \mathbf{N}^T}{\partial y} \\ \frac{\partial \mathbf{N}}{\partial y} \frac{\partial \mathbf{N}^T}{\partial x} & \frac{\partial \mathbf{N}}{\partial y} \frac{\partial \mathbf{N}^T}{\partial y} \end{pmatrix} d\Omega \\ &= \left( \sum_j \int_{\Omega} p_j'(\mathbf{x}) \begin{pmatrix} \frac{\partial \mathbf{N}}{\partial x} \frac{\partial \mathbf{N}^T}{\partial x} & \frac{\partial \mathbf{N}}{\partial x} \frac{\partial \mathbf{N}^T}{\partial y} \\ \frac{\partial \mathbf{N}}{\partial y} \frac{\partial \mathbf{N}^T}{\partial x} & \frac{\partial \mathbf{N}}{\partial y} \frac{\partial \mathbf{N}^T}{\partial y} \end{pmatrix} d\Omega q_j'(\omega) \right. \\ & \quad \left. + i \sum_j \int_{\Omega} p_j''(\mathbf{x}) \begin{pmatrix} \frac{\partial \mathbf{N}}{\partial x} \frac{\partial \mathbf{N}^T}{\partial x} & \frac{\partial \mathbf{N}}{\partial x} \frac{\partial \mathbf{N}^T}{\partial y} \\ \frac{\partial \mathbf{N}}{\partial y} \frac{\partial \mathbf{N}^T}{\partial x} & \frac{\partial \mathbf{N}}{\partial y} \frac{\partial \mathbf{N}^T}{\partial y} \end{pmatrix} d\Omega q_j''(\omega) \right) \end{aligned} \quad (33)$$

After some simplifications

$$\int_{\Omega} \lambda(\mathbf{x}, \omega) \begin{pmatrix} \frac{\partial \mathbf{N}}{\partial x} \frac{\partial \mathbf{N}^T}{\partial x} & \frac{\partial \mathbf{N}}{\partial x} \frac{\partial \mathbf{N}^T}{\partial y} \\ \frac{\partial \mathbf{N}}{\partial y} \frac{\partial \mathbf{N}^T}{\partial x} & \frac{\partial \mathbf{N}}{\partial y} \frac{\partial \mathbf{N}^T}{\partial y} \end{pmatrix} d\Omega = \sum_j \mathbf{P}_j' q_j'(\omega) + i \sum_j \mathbf{P}_j'' q_j''(\omega) \quad (34)$$

where

$$\mathbf{P}_j^{(')(''')} = \int_{\Omega} p_j^{(')(''')}(\mathbf{x}) \begin{pmatrix} \frac{\partial \mathbf{N}}{\partial x} \frac{\partial \mathbf{N}^T}{\partial x} & \frac{\partial \mathbf{N}}{\partial x} \frac{\partial \mathbf{N}^T}{\partial y} \\ \frac{\partial \mathbf{N}}{\partial y} \frac{\partial \mathbf{N}^T}{\partial x} & \frac{\partial \mathbf{N}}{\partial y} \frac{\partial \mathbf{N}^T}{\partial y} \end{pmatrix} d\Omega \quad (35)$$

In the same way we can write

$$\int_{\Omega} \mu \begin{pmatrix} 2 \frac{\partial \mathbf{N}}{\partial x} \frac{\partial \mathbf{N}^T}{\partial x} + \frac{\partial \mathbf{N}}{\partial y} \frac{\partial \mathbf{N}^T}{\partial y} & \frac{\partial \mathbf{N}}{\partial y} \frac{\partial \mathbf{N}^T}{\partial x} \\ \frac{\partial \mathbf{N}}{\partial x} \frac{\partial \mathbf{N}^T}{\partial y} & 2 \frac{\partial \mathbf{N}}{\partial y} \frac{\partial \mathbf{N}^T}{\partial y} + \frac{\partial \mathbf{N}}{\partial x} \frac{\partial \mathbf{N}^T}{\partial x} \end{pmatrix} d\Omega = \sum_j \mathbf{R}_j' s_j'(\omega) + i \sum_j \mathbf{R}_j'' s_j''(\omega) \quad (36)$$

where

$$\mathbf{R}_j^{(')(''')} = \int_{\Omega} r_j^{(')(''')}(\mathbf{x}) \begin{pmatrix} 2 \frac{\partial \mathbf{N}}{\partial x} \frac{\partial \mathbf{N}^T}{\partial x} + \frac{\partial \mathbf{N}}{\partial y} \frac{\partial \mathbf{N}^T}{\partial y} & \frac{\partial \mathbf{N}}{\partial y} \frac{\partial \mathbf{N}^T}{\partial x} \\ \frac{\partial \mathbf{N}}{\partial x} \frac{\partial \mathbf{N}^T}{\partial y} & 2 \frac{\partial \mathbf{N}}{\partial y} \frac{\partial \mathbf{N}^T}{\partial y} + \frac{\partial \mathbf{N}}{\partial x} \frac{\partial \mathbf{N}^T}{\partial x} \end{pmatrix} d\Omega \quad (37)$$

Finally, we obtain one of the most difficult terms of our variational formulation

$$\int_{\Omega} \varepsilon^{*T} \cdot \sigma \, d\Omega = \begin{pmatrix} \mathbf{u}^{*T} & \mathbf{v}^{*T} \end{pmatrix} \left( \sum_j \mathbf{P}'_j q'_j(\omega) + i \sum_j \mathbf{P}''_j q''_j(\omega) + \sum_j \mathbf{R}'_j s'_j(\omega) + i \sum_j \mathbf{R}''_j s''_j(\omega) \right) \begin{pmatrix} \mathbf{u}_x \\ \mathbf{u}_y \end{pmatrix} \quad (38)$$

Now we can move to the other terms that will be easier to develop. The inertial term is given by

$$\int_{\Omega} \rho(\mathbf{x}) V^* \ddot{\mathbf{u}} \, d\Omega = \begin{pmatrix} \mathbf{u}^{*T} & \mathbf{v}^{*T} \end{pmatrix} \left[ \int_{\Omega} \rho(\mathbf{x}) \begin{pmatrix} \mathbf{N}\mathbf{N}^T & 0 \\ 0 & \mathbf{N}\mathbf{N}^T \end{pmatrix} d\Omega \right] \begin{pmatrix} \ddot{\mathbf{u}}_x \\ \ddot{\mathbf{u}}_y \end{pmatrix} \quad (39)$$

where  $\mathbf{M}$  denotes the mass matrix and is defined as

$$\mathbf{M} = \int_{\Omega} \rho(\mathbf{x}) \begin{pmatrix} \mathbf{N}\mathbf{N}^T & 0 \\ 0 & \mathbf{N}\mathbf{N}^T \end{pmatrix} d\Omega \quad (40)$$

This matrix takes into account the variation of the densities through the layers by an appropriate definition of  $\rho(\mathbf{x})$ . Namely,

$$\rho(\mathbf{x}) = \rho_j \quad \text{for} \quad -\sum_{k=1}^j h_k < z \leq -\sum_{k=1}^{j-1} h_k \quad (41)$$

As this material property does not depend on the frequency the resulting mass matrix is given just by one term (contrarily to the previous stiffness matrix  $\mathbf{P}_j^{(')('')}$  and  $\mathbf{R}_j^{(')('')}$ ).

Finally, we need to define a boundary interpolation functions vector  $\mathbf{L}$  for the damping boundary conditions.  $\mathbf{L}$  allows to write:

$$\int_{\partial\Omega_{damp}} \eta V^* \cdot \dot{\mathbf{u}} \, d(\partial\Omega) = \begin{pmatrix} \mathbf{u}^{*T} & \mathbf{v}^{*T} \end{pmatrix} \left[ \int_{\partial\Omega_{damp}} \eta \begin{pmatrix} \mathbf{L}\mathbf{L}^T & 0 \\ 0 & \mathbf{L}\mathbf{L}^T \end{pmatrix} d(\partial\Omega_{damp}) \right] \begin{pmatrix} \dot{\mathbf{u}}_x \\ \dot{\mathbf{u}}_y \end{pmatrix} \quad (42)$$

Therefore, the damping matrix is given by

$$\mathbf{L} = \int_{\partial\Omega_{damp}} \eta \begin{pmatrix} \mathbf{L}\mathbf{L}^T & 0 \\ 0 & \mathbf{L}\mathbf{L}^T \end{pmatrix} d(\partial\Omega_{damp}). \quad (43)$$

*Remark:* It is worth pointing out that, in what will follow, we are going to use an extended matrix  $\mathbf{L}$ , the size of which is equal to the total number of degrees of freedom. Mainly, lines and columns with zero values will be added to this matrix corresponding to the degrees of freedom that does not belong to the boundary  $\partial\Omega_{damp}$ . This allows that the definition of the vector  $\begin{pmatrix} \mathbf{u}_x \\ \mathbf{u}_y \end{pmatrix}$  remains constant in the various terms of the variationnal form.

Let now  $\mathbf{F}_0$  be the vector that contains 1 on the excited DoF and zero elsewhere. This allows to write:

$$V_f^* F(t) = \begin{pmatrix} \mathbf{u}^{*T} & \mathbf{v}^{*T} \end{pmatrix} \mathbf{F}_0 \exp(i\omega t) \quad (44)$$

Finally, if we denote by  $\mathbf{U} = \begin{pmatrix} \mathbf{u}_x \\ \mathbf{u}_y \end{pmatrix}$  the total discrete degree-of-freedom vector, then we reach the following system after the simplification of the test fields from the variational formulation

$$\mathbf{M}\ddot{\mathbf{U}} + \left( \sum_j \mathbf{P}'_j q'_j(\omega) + i \sum_j \mathbf{P}''_j q''_j(\omega) + \sum_j \mathbf{R}'_j s'_j(\omega) + i \sum_j \mathbf{R}''_j s''_j(\omega) \right) \mathbf{U} - \mathbf{L}\dot{\mathbf{U}} = \mathbf{F}_0 \exp(i\omega t) \quad (45)$$

The displacement is supposed to follow the complex form

$$\mathbf{U} = \left( \mathbf{U}' + i\mathbf{U}'' \right) \exp(i\omega t) \quad (46)$$

That means that the displacement follows the excitation frequency but exhibits a delay depending on the value of  $\omega$ . Accordingly, the first and second time derivatives of this field write:

$$\dot{\mathbf{U}} = \left( -\omega\mathbf{U}'' + i\omega\mathbf{U}' \right) \exp(i\omega t) \quad (47)$$

$$\ddot{\mathbf{U}} = \left( -\omega^2\mathbf{U}' - i\omega^2\mathbf{U}'' \right) \exp(i\omega t) \quad (48)$$

We can now inject these expressions in the discrete form and simplify by  $\exp(i\omega t)$  to obtain the following complex equation:

$$\begin{aligned} & \mathbf{M} \left( -\omega^2\mathbf{U}' - i\omega^2\mathbf{U}'' \right) + \\ & \left( \sum_j \mathbf{P}'_j q'_j(\omega) + i \sum_j \mathbf{P}''_j q''_j(\omega) + \sum_j \mathbf{R}'_j s'_j(\omega) + i \sum_j \mathbf{R}''_j s''_j(\omega) \right) \left( \mathbf{U}' + i\mathbf{U}'' \right) - \\ & \mathbf{L} \left( -\omega\mathbf{U}'' + i\omega\mathbf{U}' \right) = \mathbf{F}_0 \end{aligned} \quad (49)$$

Finally, separating the real and imaginary parts of the above complex equation and then gathering the obtained two equations into one matricial system, yields:

$$\begin{pmatrix} -\omega^2\mathbf{M} + \sum_j \mathbf{P}'_j q'_j(\omega) + \sum_j \mathbf{R}'_j s'_j(\omega) & -\sum_j \mathbf{P}''_j q''_j(\omega) - \sum_j \mathbf{R}''_j s''_j(\omega) + \omega\mathbf{L} \\ \sum_j \mathbf{P}''_j q''_j(\omega) + \sum_j \mathbf{R}''_j s''_j(\omega) - \omega\mathbf{L} & -\omega^2\mathbf{M} + \sum_j \mathbf{P}'_j q'_j(\omega) + \sum_j \mathbf{R}'_j s'_j(\omega) \end{pmatrix} \begin{pmatrix} \mathbf{U}' \\ \mathbf{U}'' \end{pmatrix} = \begin{pmatrix} \mathbf{F}_0 \\ \mathbf{0} \end{pmatrix} \quad (50)$$

For a given value of  $\omega$  the obtained the system is linear. Solving this system directly gives  $\begin{pmatrix} \mathbf{U}' \\ \mathbf{U}'' \end{pmatrix}$ . It is also possible to make the matrix of the above system symmetric by multiplying the second line by (-1).

### Remark

In order to post-process the results we are going to extract from the solution  $\begin{pmatrix} \mathbf{U}' \\ \mathbf{U}'' \end{pmatrix}$  some significant values (this will be also the case for post processing each mode of the PGD results of the following sections)  
Let denotes by  $(\mathbf{U}'_x, \mathbf{U}'_y, \mathbf{U}'_z)$  (resp.  $(\mathbf{U}''_x, \mathbf{U}''_y, \mathbf{U}''_z)$ ) the three components of  $\mathbf{U}'$  (resp. of  $\mathbf{U}''$ ). We can then define an amplitude gain along each axes by

$$\mathbf{A}_x = \sqrt{\mathbf{u}'_x{}^2 + \mathbf{u}''_x{}^2} \quad (51)$$

$$\mathbf{A}_y = \sqrt{\mathbf{u}'_y{}^2 + \mathbf{u}''_y{}^2} \quad (52)$$

$$\mathbf{A}_z = \sqrt{\mathbf{u}'_z{}^2 + \mathbf{u}''_z{}^2} \quad (53)$$

We also can define an angular phase according to

$$\phi_x = \text{atan}(\mathbf{u}''_x / \mathbf{u}'_x) \quad (54)$$

$$\phi_y = \text{atan}(\mathbf{u}''_y / \mathbf{u}'_y) \quad (55)$$

$$\phi_z = \text{atan}(\mathbf{u}''_z / \mathbf{u}'_z) \quad (56)$$

Finally it is possible to make a regeneration of the time dependent solution according to

$$\mathbf{U}(t) = \mathbf{U}' \cos(\omega t) - \mathbf{U}'' \sin(\omega t) \quad (57)$$

## 4 Model reduction using PGD decomposition

### 4.1 Without material parameters uncertainty

As stated before, the size of the finite-element problem is large. Sometimes, it is important to bounded soil domain. It is also important to undertake a parametric study. However, the size of the finite-element problem is prohibitive for such study. In order reduce the size of the numerical model and make computation times reasonable, the numerical model will be here solved within the framework of the PGD (Proper Generalized Decomposition) method. The PGD is a numerical technique that allows circumventing the curse of dimensionality in the resolution of a high dimensional problem [51, 52, 53, 54, 55, 56, 57]. Especially, the case of parametric study could be found in [58, 59, 60]. **Following Malick et al. [49] and Germoso et al. [48] the elastodynamic problem is formulated in the frequency-space domain. The PGD method is then used to solve the elastodynamic problem considering the frequency as an extra coordinate.**

In our case we are going to apply such an idea for solving the problem assuming that the value of  $\omega$  is unknown. This is possible only because the frequency and space variables are independent, which is a main advantage of the frequency-space formulation. Indeed, it will be less evident to use the PGD method in a time-space formulation as the time variable and space variable are linked in wave propagation problems through characteristic equations.

In order to prepare a kind of general solution in which the displacement field will depends on the position as well as on the value of  $\omega$  we must write the problem as:

$$\mathbf{A}\mathbf{U} = \mathbf{B}, \quad (58)$$

where

$$\mathbf{A} = \sum_{j=1}^{n_A} \mathbf{A}_x^j \otimes \mathbf{A}_\omega^j \otimes \mathbf{A}_c^j \quad (59)$$

and

$$\mathbf{B} = \sum_{j=1}^{n_b} \mathbf{B}_x^j \otimes \mathbf{B}_\omega^j \otimes \mathbf{B}_c^j. \quad (60)$$

Here  $\mathbf{A}_x^j$  (resp.  $\mathbf{B}_x^j$ ) are operators (resp. vectors) of the three coordinate physical space  $\mathbf{x}$ ,  $\mathbf{A}_\omega^j$  (resp.  $\mathbf{B}_\omega^j$ ) are operators (resp. vectors) of the frequential space,  $\mathbf{A}_c^j$  (resp.  $\mathbf{B}_c^j$ ) are operators (resp. vectors) of a 2 DoF complex space, the first coordinate is the real axis and the second one is the imaginary one.  $\otimes$  stands for the tensor product operator.

The solutions are searched in the following form

$$\mathbf{U} = \sum_{j=1}^{n_u} \mathbf{f}_x^j \otimes \mathbf{f}_\omega^j \otimes \mathbf{f}_c^j, \quad (61)$$

where  $\mathbf{f}_c^j = c'^j + ic''^j$ . In order to apply the tensor product resolution technique to find  $\mathbf{U}$  we have just to give the tensor form of operators  $\mathbf{A}$  and  $\mathbf{B}$ . The greedy algorithm for building the solution  $\mathbf{U}$  is quickly and is explained in the appendix. Using the following notations:

$$\mathbf{W}_2 = \text{diag}(-\omega^2), \quad (62)$$

$$\mathbf{W}_1 = \text{diag}(\omega), \quad (63)$$

$$\mathbf{Q}_j^{(')(''')} = \text{diag}\left(q_j^{(')(''')}(\omega)\right), \quad (64)$$

and

$$\mathbf{S}_j^{(')(''')} = \text{diag}\left(s_j^{(')(''')}(\omega)\right), \quad (65)$$

where  $\text{diag}$  is the operator that build a diagonal matrice from all the discrete values of the included function applied individually on each discrete value of  $\omega$ ,

the system of Eq. (49) becomes defined by

$$\begin{aligned} \mathbf{A} = & \mathbf{M} \otimes \mathbf{W}_2 \otimes \begin{pmatrix} 1 & 0 \\ 0 & 1 \end{pmatrix} + \sum_j \mathbf{P}'_j \otimes \mathbf{Q}'_j \otimes \begin{pmatrix} 1 & 0 \\ 0 & 1 \end{pmatrix} \\ & + \sum_j \mathbf{R}'_j \otimes \mathbf{S}'_j \otimes \begin{pmatrix} 1 & 0 \\ 0 & 1 \end{pmatrix} + \sum_j \mathbf{P}''_j \otimes \mathbf{Q}''_j \otimes \begin{pmatrix} 0 & -1 \\ 1 & 0 \end{pmatrix} \\ & + \sum_j \mathbf{R}''_j \otimes \mathbf{S}''_j \otimes \begin{pmatrix} 0 & -1 \\ 1 & 0 \end{pmatrix} + \mathbf{L} \otimes \mathbf{W}_1 \otimes \begin{pmatrix} 0 & 1 \\ -1 & 0 \end{pmatrix} \end{aligned} \quad (66)$$

which is already under the desired form of Eq. (59) and also by

$$\mathbf{B} = \mathbf{F}_0 \otimes \begin{pmatrix} 1 \\ \vdots \\ 1 \end{pmatrix} \otimes \begin{pmatrix} 1 \\ 0 \end{pmatrix} \quad (67)$$

which is already under the desired form of Eq. (60).

The PGD solver provide the solution as detailed in the Appendix:

$$\mathbf{U} = \mathbf{A} \setminus \mathbf{B} = \sum_{j=1}^{n_u} \mathbf{f}_x^j \otimes \mathbf{f}_\omega^j \otimes \mathbf{f}_c^j. \quad (68)$$

And by post processing we obtain:

$$\mathbf{U}' = \sum_{j=1}^{n_u} \mathbf{f}_x^j \otimes \mathbf{f}_\omega^j \otimes \mathbf{c}'^j, \quad (69)$$

and

$$\mathbf{U}'' = \sum_{j=1}^{n_u} \mathbf{f}_x^j \otimes \mathbf{f}_\omega^j \otimes \mathbf{c}''^j. \quad (70)$$

We also can rewrite again the solution as

$$\mathbf{U} = \sum_{j=1}^{n_u} \mathbf{U}^j \otimes \mathbf{f}_\omega^j, \quad (71)$$

where  $\mathbf{U}^j$  are the modes obtained by

$$\mathbf{U}^j = \mathbf{f}_x^j \otimes \mathbf{c}'^j + \mathbf{f}_x^j \otimes \mathbf{c}''^j. \quad (72)$$

## 4.2 With material parameters uncertainty

The soil parameters are not well defined. It is important to analyze the response of the layered soil considering that the parameters may vary within a certain range. The computational cost of this type of study is quite prohibitive unless model reduction techniques are used as the elastodynamic problem should

be solved multiple times while varying the material parameter within the desired range. Within the framework of the PGD decomposition, it is possible to consider that each material parameter is a variable playing similar role in the decomposition than the space variable  $\mathbf{x}$  and the frequency  $\omega$ .

For sake of clarity, we are going to formulate the parametric problem for a soil with two layers. The procedure remains the same for a different parameterization or higher number of layer. As for Section 4.1, the problem is written as follows:

$$\mathbf{A}\mathbf{U} = \mathbf{B} \quad (73)$$

where

$$\mathbf{A} = \sum_{j=1}^{n_A} \mathbf{A}_x^j \otimes \mathbf{A}_c^j \otimes \mathbf{A}_{E_1}^j \otimes \mathbf{A}_{E_2}^j \quad (74)$$

$$\mathbf{B} = \sum_{j=1}^{n_b} \mathbf{B}_x^j \otimes \mathbf{B}_c^j \otimes \mathbf{B}_{E_1}^j \otimes \mathbf{B}_{E_2}^j \quad (75)$$

$\mathbf{A}_x^j$  (resp  $\mathbf{B}_x^j$ ) are operators (resp vectors) related to three coordinate physical space  $\mathbf{x}$ , and  $\mathbf{A}_c^j$  (resp  $\mathbf{B}_c^j$ ) are operators (resp vectors) related to the 2DoF complex space, the first coordinate is the real axis and the second one is the imaginary one. Also,  $\mathbf{A}_{E_1}^j$  (resp  $\mathbf{B}_{E_1}^j$ ) are operators (resp vectors) related to the parametric coordinate  $E_1$ , and  $\mathbf{A}_{E_2}^j$  (resp  $\mathbf{B}_{E_2}^j$ ) are operators (resp vectors) related to the parametric coordinate  $E_2$ .

We will look to the solution as

$$\mathbf{U} = \sum_{j=1}^{n_u} \mathbf{f}_x^j \otimes \mathbf{f}_c^j \otimes \mathbf{f}_{E_1}^j \otimes \mathbf{f}_{E_2}^j \quad (76)$$

$$\mathbf{f}_c^j = c'^j + ic''^j \quad (77)$$

In order to apply the tensor product resolution technique to find  $\mathbf{U}$  we just have to give the tensor form of operators  $\mathbf{A}$  and  $\mathbf{B}$ . The greedy algorithm for building the solution  $\mathbf{U}$  is explained in the appendix.

We use the following notations (where *diag* is the operator that build a diagonal matrix from all the discrete values of  $E_{1,2}$ )

$$\mathbf{E}_1 = \text{diag}(E_1) \quad (78)$$

$$\mathbf{E}_2 = \text{diag}(E_2) \quad (79)$$

Moreover,  $\mathbf{1}_{E_1}$  the identity matrix of size equal to the number of discrete values of  $E_1$  and  $\mathbf{1}_{E_2}$  the identity matrix of size equal to the number of discrete values of  $E_2$ .

The operator  $\mathbf{A}$  writes:

$$\begin{aligned}
\mathbf{A} = & \mathbf{M} \otimes \begin{pmatrix} -1 & 0 \\ 0 & 1 \end{pmatrix} \otimes \mathbf{1}_{E_1} \otimes \mathbf{1}_{E_1} + \mathbf{L} \otimes \begin{pmatrix} 0 & 1 \\ 1 & 0 \end{pmatrix} \otimes \mathbf{1}_{E_1} \otimes \mathbf{1}_{E_1} \\
& + \left( (\mathbf{P}'_1 q'_1) + (\mathbf{R}'_1 s'_1) \right) \otimes \begin{pmatrix} 1 & 0 \\ 0 & -1 \end{pmatrix} \otimes \mathbf{E}_1 \otimes \mathbf{1}_{E_2} \\
& + \left( (\mathbf{P}'_2 q'_2) + (\mathbf{R}'_2 s'_2) \right) \otimes \begin{pmatrix} 1 & 0 \\ 0 & -1 \end{pmatrix} \otimes \mathbf{1}_{E_1} \otimes \mathbf{E}_2 \\
& + \left( (\mathbf{P}''_1 q''_1) + (\mathbf{R}''_1 s''_1) \right) \otimes \begin{pmatrix} 0 & -1 \\ -1 & 0 \end{pmatrix} \otimes \mathbf{E}_1 \otimes \mathbf{1}_{E_2} \\
& + \left( (\mathbf{P}''_2 q''_2) + (\mathbf{R}''_2 s''_2) \right) \otimes \begin{pmatrix} 0 & -1 \\ -1 & 0 \end{pmatrix} \otimes \mathbf{1}_{E_1} \otimes \mathbf{E}_2
\end{aligned} \quad , \quad (80)$$

which is already under the form of Eq. (59); whereas, the right-hand operator  $\mathbf{B}$  writes:

$$\mathbf{B} = \mathbf{F}_0 \otimes \begin{pmatrix} 1 \\ 0 \end{pmatrix} \otimes \begin{pmatrix} 1 \\ \vdots \\ 1 \end{pmatrix} \otimes \begin{pmatrix} 1 \\ \vdots \\ 1 \end{pmatrix}, \quad (81)$$

which is already under the form of Eq. (60).

Our PGD solver provide the solution (see the appendix)

$$\mathbf{U} = \mathbf{A} \setminus \mathbf{B} = \sum_{j=1}^{n_u} \mathbf{f}_x^j \otimes \mathbf{f}_c^j \otimes \mathbf{f}_{E_1}^j \otimes \mathbf{f}_{E_2}^j. \quad (82)$$

We also can (if we want) rewrite again the solution as

$$\mathbf{U} = \sum_{j=1}^{n_u} \mathbf{U}^j \otimes \mathbf{E}^j \quad (83)$$

Where  $\mathbf{U}^j$  are the modes obtained by

$$\mathbf{U}^j = \mathbf{f}_x^j \otimes c'^j + \mathbf{f}_x^j \otimes c''^j \quad (84)$$

and  $\mathbf{E}^j$  are the combinations of the two 1D parametric modes into the one 2D parametric space

$$\mathbf{E}^j = \mathbf{f}_{E_1}^j \otimes \mathbf{f}_{E_2}^j \quad (85)$$

## 5 Results and discussion

We consider in this result section a two-layer soil domain represented in Figure 3. The unit system used for forces, lengths, densities, and stresses is the SI system. The first and second layer are 5-m and 20-m thick, respectively. The radius of the bounded is considered  $L = 50$  m. The two layers are assumed to have the same density  $\rho_{1,2} = 1980$  kg/m<sup>3</sup> and the same Poisson's ratio  $\nu_{1,2} = 0.4903$ . The Young's modulus of the first and second layer are 446 MPa and 250 MPa,

respectively. The damping ratio for the first and second layer are 0.042 and 0.039, respectively. To prevent wave reflections at the virtual boundaries, a dynamic viscosity of  $\eta = 10^8$  is considered. The harmonic force is defined by  $F(t) = F_0 \exp(i\omega t)$  where  $F_0 = 1\text{N}$ . The investigated frequency range is  $\omega = 2\pi \cdot 50$  Hz.

Thus, we can define the functions  $q'_{1,2}$ ,  $q''_{1,2}$ ,  $s'_{1,2}$ ,  $s''_{1,2}$  using:

$$\lambda_{1,2} = \frac{E_{1,2}\nu_{1,2}}{(1 - 2\nu_{1,2})(1 + \nu_{1,2})}, \quad \mu_{1,2} = \frac{E_{1,2}}{2(1 + \nu_{1,2})} \quad (86)$$

And we consider constant values of the frequential functions

$$q'_j(\omega) = \lambda_j \quad (87)$$

$$q''_j(\omega) = 0.042 \lambda_j \quad (88)$$

$$s'_j(\omega) = \mu_j \quad (89)$$

$$s''_j(\omega) = 0.039 \mu_j \quad (90)$$

Even if for the sake of simplicity these functions are taken constant in this application nothing prevents to make them frequency dependent. The reader can for example looks for such function as the real and complex modulus of the Maxwell visco-elastic model given by

$$q'_j(\omega) = G' \frac{\omega^2 \theta_j^2}{1 + \omega^2 \theta_j^2} \quad (91)$$

$$q''_j(\omega) = G'' \frac{\omega \theta_j}{1 + \omega^2 \theta_j^2} \quad (92)$$

Similar expression could be used for  $s'_j(\omega)$  and  $s''_j(\omega)$ . But this requires an experimental identification of the model parameters  $G'$ ,  $G''$  and the relaxation time  $\theta_j$ .

## 5.1 Example of non parametric results emphasizing the interest of the frequential formulation of Eq. (50)

The harmonic force is defined on various depths and could be vertical (along  $z$  direction) or horizontal (along  $x$  direction). The only symmetry plane of the problem is the plane defined by  $y = 0$ . Eight cases are investigated and are detailed in Table 1.

Figure 3, shows the position of some points on which we have plot the time dependent displacement.

Figures 4 and 5 depict the horizontal and vertical displacements, respectively, in the selected points. The displacement is important in the closest point to the applied force and in the same direction as it. The displacement almost vanishes elsewhere. Hence, Figures 4(a), 4(c), 4(e) and 4(g) corresponding to the cases 1,

Case	$x$ coordinate of the force	$y$ coordinate of the force	$z$ coordinate of the force	Direction of the force
1	0	0	0	$x$
2	0	0	0	$z$
3	0	0	-2.5	$x$
4	0	0	-2.5	$z$
5	0	0	-5	$x$
6	0	0	-5	$z$
7	0	0	-10	$x$
8	0	0	-10	$z$

Table 1: The eight studied cases

3, 5 and 7, respectively, show the dominance of the horizontal displacements of points 1, 7, 8 and 9, which are the closest to the respective points where the force is applied. Likewise, Figures 5(b), 5(d), 5(f) and 5(h) corresponding to the cases 2, 4, 6 and 8, respectively, show the dominance of the vertical displacements of points 1, 7, 8 and 9, which are the closest to the respective points where the force is applied. However, Figures 4(b), 4(d), 4(f) and 4(h) corresponding to the cases 2, 4, 6 and 8, respectively, show that the vertical displacements vanish as the corresponding forces are applied in the perpendicular horizontal direction. However, Figures 5(a), 4(c), 4(e) and 4(g) corresponding to the cases 1, 3, 5 and 7, respectively, show that the horizontal displacements vanish as the corresponding forces are applied in the perpendicular vertical direction.

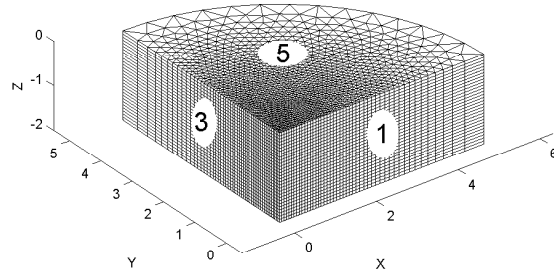
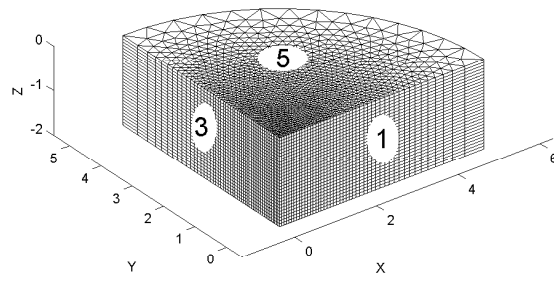


Figure 2: Geometry of the studied problem

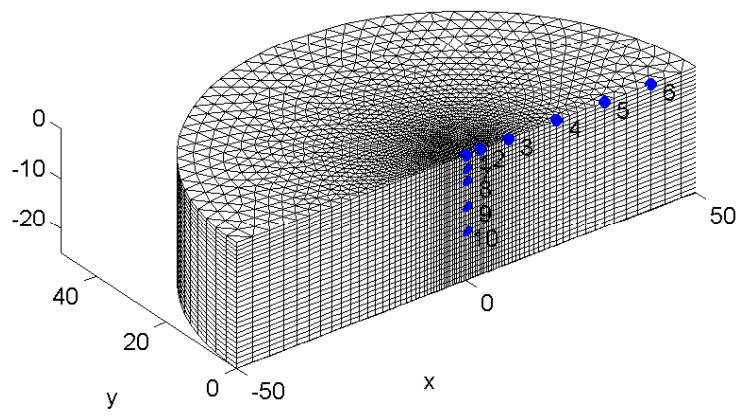
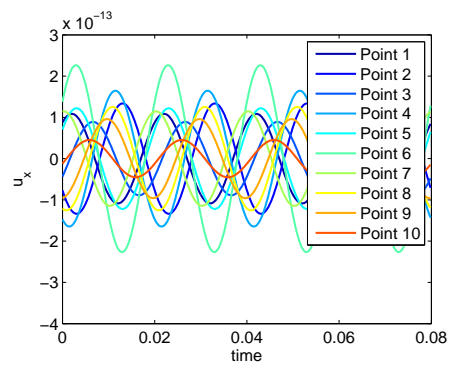
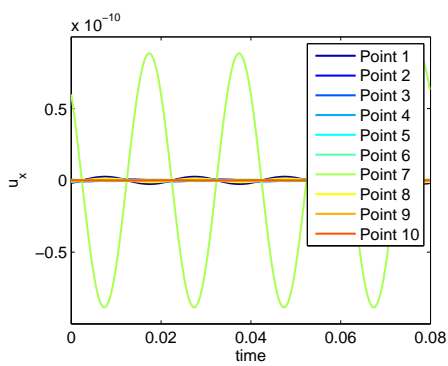
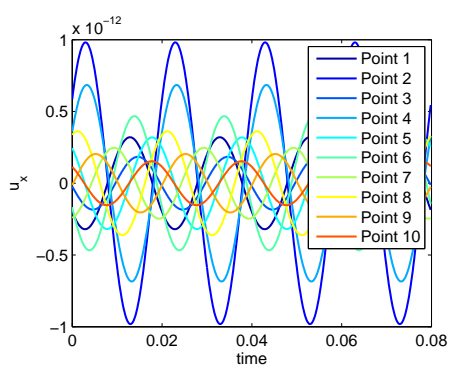
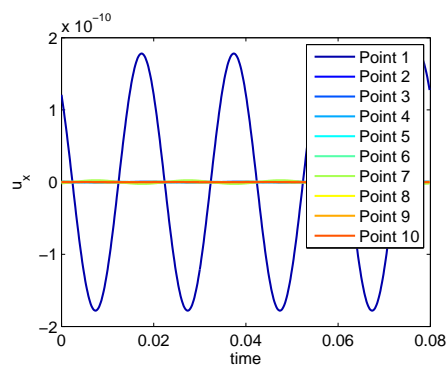


Figure 3: Position of points where the displacement response will be observed



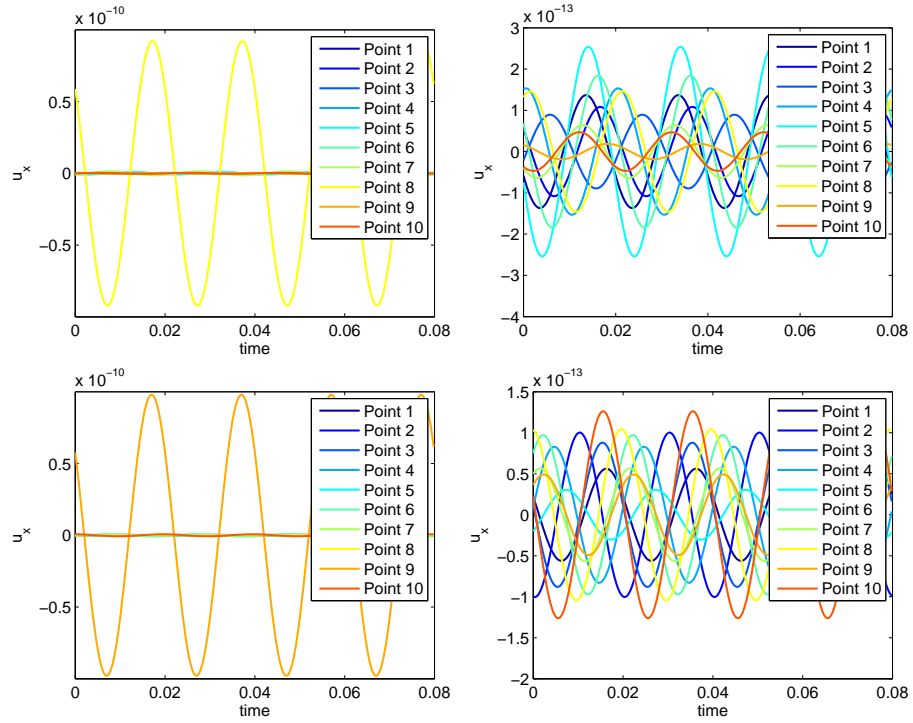
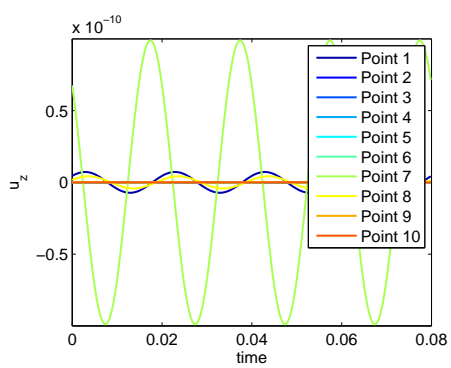
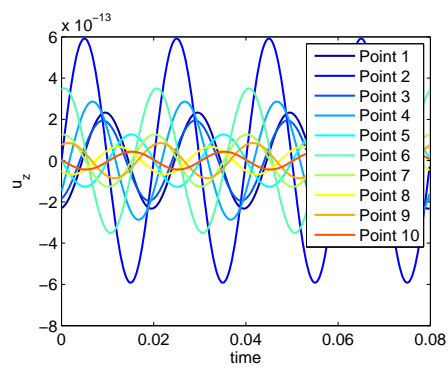
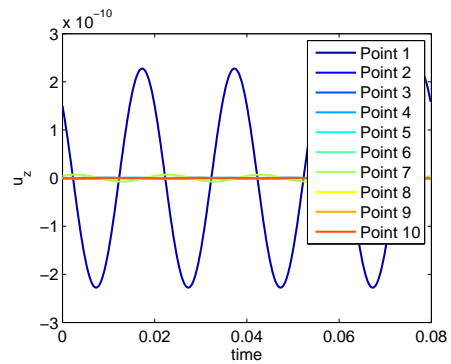
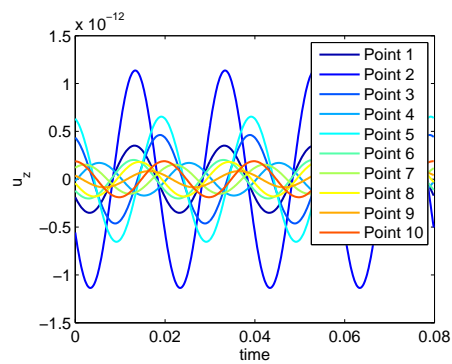


Figure 4: Horizontal displacement: (a) Case 1, (b) Case 2, (c) Case 3, (d) Case 4, (e) Case 5, (f) Case 6, (g) Case 7, and (h) Case 8



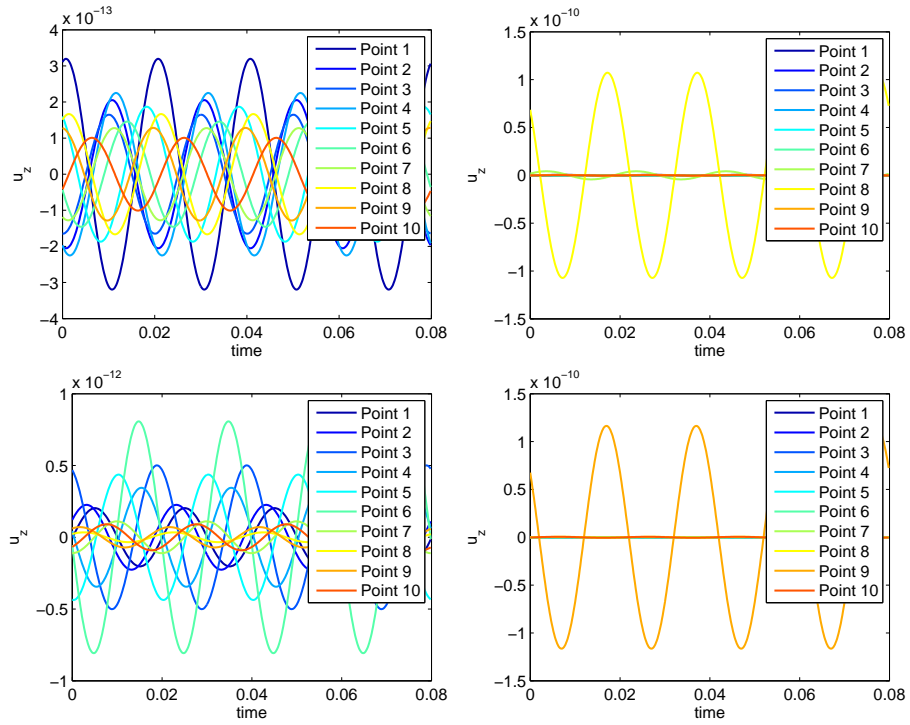


Figure 5: Vertical displacement: (a) Case 1, (b) Case 2, (c) Case 3, (d) Case 4, (e) Case 5, (f) Case 6, (g) Case 7, and (h) Case 8

## 5.2 Illustration of the PGD resolution with material parameters uncertainty

An example of result of the tensor form established in equations 24-25 is given in Figures 6-9. The harmonic force is defined by an horizontal force  $F(t) = F_0 \exp(i\omega t)$  with  $\omega = 2\pi \cdot 50$ . We consider that for each layer we have different possible values for young modulus

$$E_1 \in [350 \cdot 10^6, 450 \cdot 10^6], E_2 = [200 \cdot 10^6, 300 \cdot 10^6] \quad (93)$$

The figure 6 represents the decrease of the weight of the modes. This information is very useful for the comparison of the PGD solution to the full grid solution of the same resolution (using the full tensor product of the FE operators by the material operators). In fact the decrease of the relative value of weight of the ' $n^{th}$ ' enrichment related to the first one implicitly represents the relative *decrease of the error* of the PGD in relation to the full grid solution. This is the indicator used to estimate the convergence of the PGD solution during the successive enrichments.

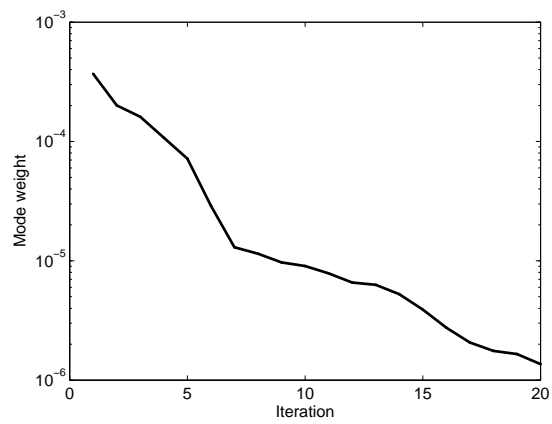


Figure 6: Decrease of the modes weight during the PGD enrichment.

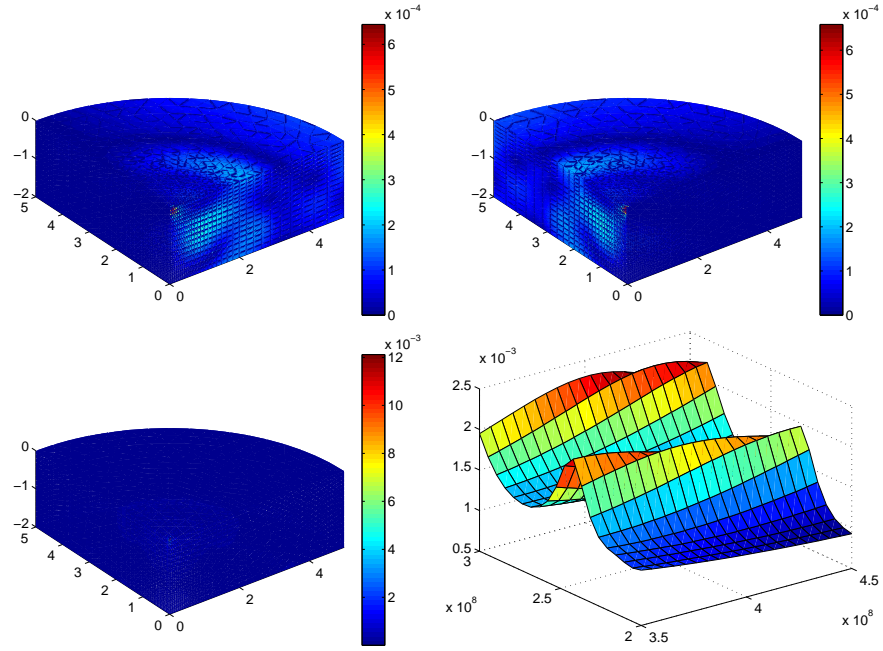


Figure 7: Mode number 1 - Space mode represented in terms of gains and parametric mode in the space (E1, E2)

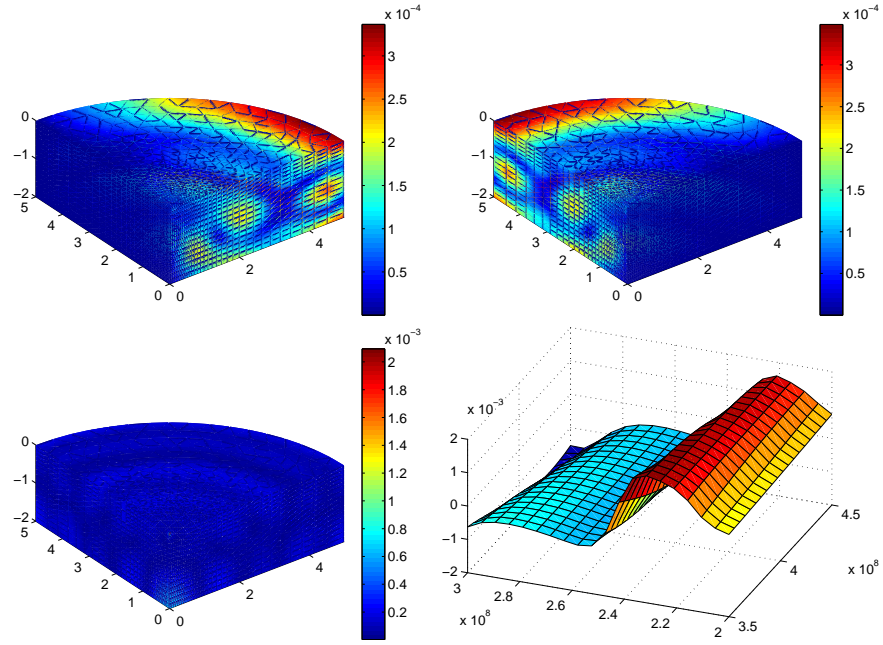


Figure 8: Mode number 2 - Space mode represented in terms of gains and parametric mode in the space (E1, E2)

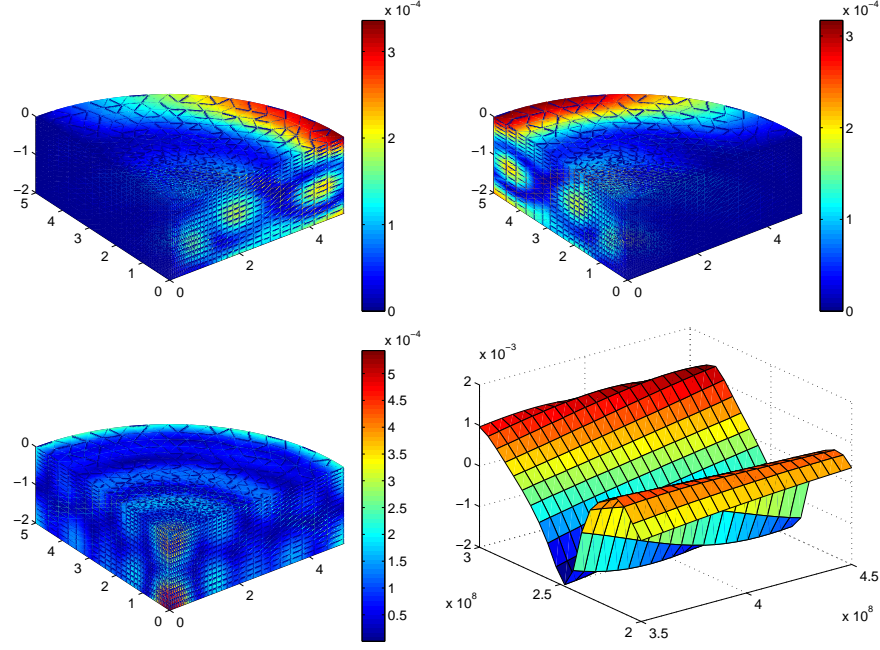


Figure 9: Mode number 3 - Space mode represented in terms of gains and parametric mode in the space ( $E_1$ ,  $E_2$ )

The functions  $\mathbf{U}^j$  and their associated  $\mathbf{E}^j$  are represented in terms of gain for the first three modes in figures 7-9. The interest of such a representation is mainly to obtain an offline solution. When the user gives the value of  $E_1$  and  $E_2$  then the results comes defined by a linear combination of modes according to

$$\mathbf{U} = \sum_{j=1}^{n_u} \alpha^j \mathbf{U}^j, \quad \alpha^j = \mathbf{E}^j(E_1, E_2) \quad (94)$$

To emphasize on the time saving obtained by using the PGD method in this case we consider the example where the material parameters are considered as parametric dimensions. Let's take the case where we are interested on problem involving  $n_{E_1}$  points in the parametric axis of  $E_1$  and  $n_{E_2}$  points in the parametric axis of  $E_2$ . In classical resolution to cover all this space we need  $n_{E_1} \cdot n_{E_2}$  resolutions of the linear system (Eq. (50)) that involves  $6N$  degrees of freedom where  $N$  is the number of nodes. When the PGD is used we have a set of linear system to solve at each iteration of the fixed-point strategy defined by the equation A.16 related to each dimension. The operator of this equation is defined in A.13 and has a size equal to

1.  $3N$  : for the first dimension (which is the spatial dimension)
2. 2 for the second dimension

3.  $n_{E_1}$  for the third dimension
4.  $n_{E_2}$  for the fourth dimension

In that case the system that will determine the CPU time will be the one related to the spatial dimension. All the other resolutions can be neglected in relation to this one. In general, the fixed point converges in about 5 iterations and the enrichment strategy reaches the global convergence criteria (A.17) within about 10 enrichments. Thus the global cost of the PGD can be estimated to 50 resolutions of  $3N$  dof linear system. This cost is generally much lower than  $n_{E_1} \cdot n_{E_2}$  resolutions of  $6N$  dof linear system. But this is not the only advantage of the PGD decomposition. In that case, the PGD resolution allows providing an off-line solution, i.e. a solution that is calculated only once. When the user precise the parameters values the particularization of the solution can be done in real time. This benefit opens up a lot of prospects for touch app development on smartphones for example.

### 5.3 Illustration of the PGD resolution where the frequency is considered as parameter

With the same parameters previously used we work now with PGD decomposition where material parameters are fixed but where frequency is considered as a parameter (see Eq. 21-22). An example of result is given in figure 10 and 11.

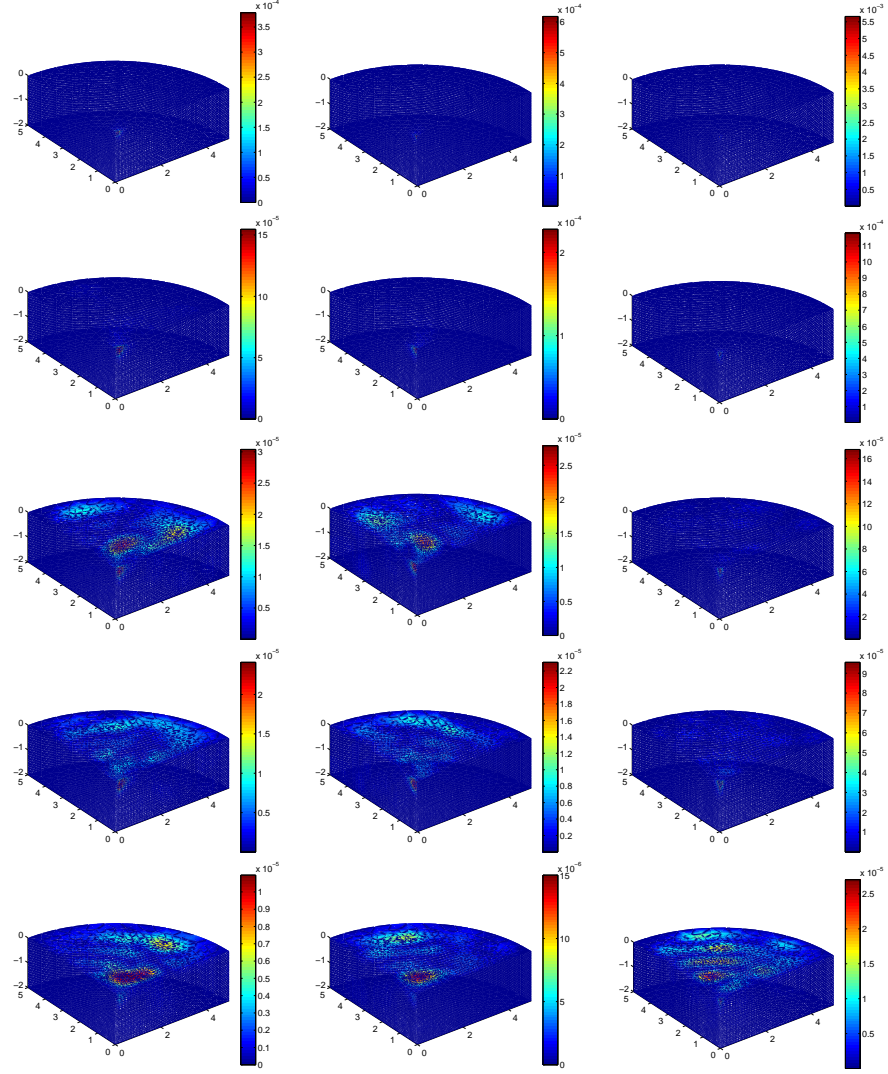


Figure 10: PGD representation of the frequency parametric solution. From top to down: the  $U^j$  functions associated to the fifth first modes ( $j = 1..5$ ). For each mode we show the three gains along X, Y and Z (on each column)

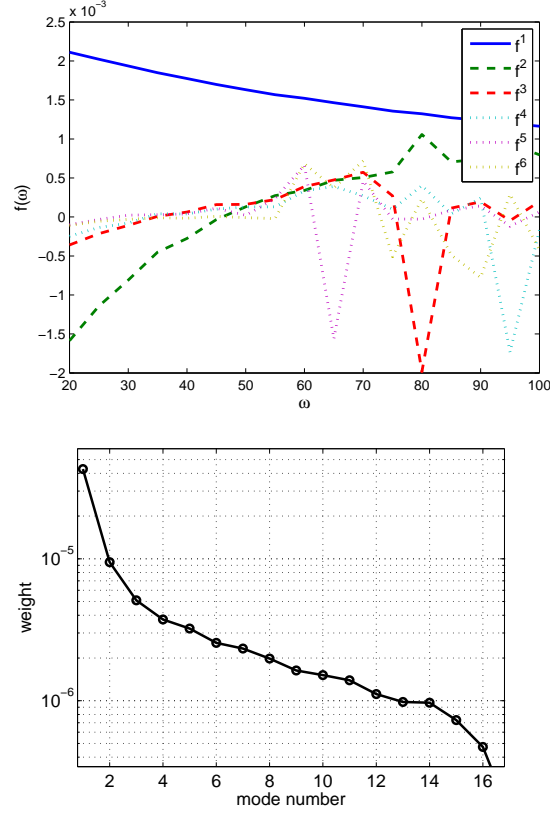


Figure 11: PGD representation of the frequency parametric solution. On the left we the frequency modes associated to those of figure 10.a. On the right we plot the weight of each mode.

The functions  $\mathbf{U}^j$  are represented in terms of gain for the first four modes in figure 10. In figure 11 we represent  $\mathbf{f}_{\omega}^{j=1..6}$ . The interest of such a representation is mainly to obtain an offline solution. When the user precise the particular value of  $\omega = \omega_p$  then the results comes defined by a linear combination of modes according to

$$\mathbf{U} = \sum_{j=1}^{n_u} \alpha^j \mathbf{U}^j, \quad \alpha^j = \mathbf{f}_{\omega}^j(\omega_p) \quad (95)$$

As for the previous case the right plot in figure 11 represents the decrease of the weight of the modes, useful information for estimating the convergence of the PGD successive enrichments.

**Remark:** The different PGD functions  $\mathbf{U}^j$  (which are sometimes called modes) do not actually represent the modes relating to a given frequency. But the solution sought for each frequency is a linear combination of these different

functions using the factors  $\mathbf{f}_{\omega}^j(\omega_p)$ .

## 6 Conclusion

In this work, we propose a general 3D framework able to give the harmonic response of exited visco-elastic soil within a space-frequency formulation. This formulation allows getting the harmonic solution without any explicit or implicit time integration scheme. 3D results show that we are able to characterize the response for a given frequency in terms of gain, angular phase and reconstituted time dependent displacement field. Displacement of points of interest in our structure (such are points on which constraints on displacement may be imposed) can be accurately represented during time in order to quantify their associated amplitude. The PGD method was also successfully formulated and validated in the frequency-space domain. It can be used for the parametric study where the frequency is a priori unknown. Finally, this new approach allows for a parametric study with a reasonable time computation cost.

## 7 Acknowledgement

This work was supported by the Deanship of Scientific Research (DSR), King Abdulaziz University, Jeddah, under the grant No. (D1439-40-135). The authors, therefore, gratefully acknowledge the DSR technical and financial support.

## References

- [1] G. Degrande, D. Clouteau, R. Othman, M. Arnst, H. Chebli, R. Klein, P. Chatterjee, B. Janssens. A numerical model for ground-borne vibrations from underground railway traffic based on a periodic finite element–boundary element formulation. *J. Sound Vib.*, 293, 645-666, 2006.
- [2] H. Chebli, R. Othman, D. Clouteau, M. Arnst, G. Degrande. 3D periodic BE–FE model for various transportation structures interacting with soil. *Comput. Geotech.*, 35, 22–32, 2008.
- [3] D. Brookes, W.I. Hamad, J.P. Talbot, H.E.M. Hunt, M.F.M. Hussein. The dynamic interaction effects of railway tunnels: Crossrail and the Grand Central Recording Studios. *Proc. Inst. Mech. Eng., Part F: J. Rail Rapid Transit*, 232(2), 542-559, 2018.
- [4] L. Fryba. *Vibrations of solids and structures under moving loads*, Thomas Telford Ed., 1999.
- [5] M. Germonpré, J.C.O. Nielsen, G. Degrande, G.Lombaert. Contributions of longitudinal track unevenness and track stiffness variation to railway induced vibration. *J. Sound Vib.* 437, 292-307, 2018.

- [6] Y. B. Yang, H. H. Hung. Soil vibrations caused by underground moving trains. *J. Geotech. Geoenviron. Eng.*, 134, 1633–1644, 2008.
- [7] S. Gupta, M. F. M. Hussein, G. Degrande, H. E. M. Hunt, D. Clouteau. A comparison of two numerical models for the prediction of vibrations from underground railway traffic. *Soil Dyn. Earthquake Eng.* 27, pp. 608–624, 2007.
- [8] X. Sheng, C. J. C. Jones, D. J. Thompson. Modelling ground vibration from railways using wavenumber finite- and boundary-element methods. *Proc. Roy. Soc. A – Math. Phys. Eng. Sci.*, 461, 2043–2070, 2005.
- [9] L. Andersen, C. J. C. Jones. Coupled boundary and finite element analysis of vibration from railway tunnels-a comparison of two- and three-dimensional models. *J. Sound Vib.*, 293, 611–625, 2006.
- [10] X. Zhang, S. Zhou, H. Di, C. He. A semi-analytical model of the train-floating slab track-tunnel-soil system considering the non-linear wheel/rail contact. *Proc. Inst. Mech. Eng., Part F: J. Rail Rapid Transit*, 232, 2063–2078, 2018.
- [11] C. He, S. Zhou, H. Di, P. Guo, J., Xiao. Analytical method for calculation of ground vibration from a tunnel embedded in a multi-layered half-space. *Comput. Geotech.*, 99, 149–164, 2018.
- [12] C. He, S. Zhou, P. Guo, H. Di, X. Zhang. Analytical model for vibration prediction of two parallel tunnels in a full-space. *J. Sound Vib.*, 423, 306–321, 2018.
- [13] C. He, S. Zhou, P. Guo, H. Di, X. Yang. A three-dimensional semi-analytical method for calculating vibrations from a moving load on a periodic jointed tunnel. *Comput. Geotech.* 2019.
- [14] Z. Yuan, Z. Cao, A. Boström, Y. Cai. The influence of pore-fluid in the soil on ground vibrations from a tunnel embedded in a layered half-space. *J. Sound Vib.*, 419, 227–248, 2018.
- [15] Q. Jin, D.J. Thompson, D.E.J. Lurcock, M.G.R. Toward, E.A. Ntotsios. A 2.5D finite element and boundary element model for the ground vibration from trains in tunnels and validation using measurement data. *J. Sound Vib.*, 422, 373–389, 2018.
- [16] Y.B. Yang, P. Ge, Q., Li, X., Liang, Y., Wu. 2.5D vibration of railway-side buildings mitigated by open or infilled trenches considering rail irregularity. *Soil Dyn. Earthquake Eng.*, 106, 204–214, 2018.
- [17] Q. Feng, S., Liu, X., Lei. Preliminary analysis of the interaction between tunnel and soil by the 2.5d fem-bem method. *Environ. Vib. Transp. Geodyn.*, 2016, 411–432, 2018.

- [18] A. Yaseri, M.H., Bazyar, S., Javady. 2.5D coupled FEM-SBFEM analysis of ground vibrations induced by train movement. *Soil Dyn. Earthquake Eng.*, 104, 307-318, 2018.
- [19] L. Godinho, D. Jr. Soares. Numerical simulation of soil-structure elastodynamic interaction using iterative-adaptive BEM-FEM coupled strategies. *Eng. Analysis Boundary Elements*, 82, 141-161, 2017.
- [20] C. He, S. Zhou, H. Di, Y. Shan. A 2.5-D coupled FE-BE model for the dynamic interaction between saturated soil and longitudinally invariant structures. *Comput. Geotech.*, 82, 211-222, 2017.
- [21] D. Clouteau D. Aubry, M.L. Elhabre. Periodic BEM and FEM-BEM coupling: applications to seismic behaviour of very long structures. *Comput. Mech.*, 25, 567-577, 2000.
- [22] H. Chebli, R. Othman, D. Clouteau. Response of periodic structures due to moving loads. *C. R. Mecanique*, 334, 347-352, 2006.
- [23] H. Chebli, D. Clouteau, L. Schmitt. Dynamic response of high-speed ballasted railway tracks: 3D periodic model and in situ measurements. *Soil Dyn. Earthquake Eng.* 28, 118-131, 2008.
- [24] M. Arnst, D. Clouteau, H. Chebli, R. Othman, G. Degrande. A non-parametric probabilistic model for ground-borne vibrations in buildings. *Prob. Eng. Mech.*, 21, 18-34, 2006.
- [25] A. Strukelj, T. Plibersek, A. Umek. Evaluation of Green's-function for vertical pointload excitation applied to the surface of a layered semi-infinite elastic medium. *Arch. Appl. Mech.*, 76, 465-479, 2006.
- [26] J. Miklowitz. *The Theory of Elastic Waves and Waveguides*. North-Holland, Amsterdam, 1980.
- [27] M. Premrov, I. Spacapan. Solving exterior problems of wave propagation based on an iterative variation of local DtN operators. *Appl. Math. Model.*, 28, 291-304, 2004.
- [28] E. Kausel. An explicit solution for the Green's-function for dynamic loads in layered media. Research Report R81-13, Massachusetts Institute of Technology, 1981.
- [29] A.V. Vostroukhov, S.N. Verichev, A.W.M. Kok, C. Esveld. Steady-state response of a stratified half-space subjected to a horizontal arbitrary buried uniform load applied at a circular area. *Soil Dyn. Earthq. Eng.*, 24, 449-459, 2004.
- [30] R.Y.S. Pak, B.B. Guzina. Three-dimensional Green's-functions for a multi-layered half-space in displacement potentials. *J. Eng. Mech.*, 128, 449-461, 2002.

- [31] C.D. Wang, C.S. Tzeng, E. Pan, J.J. Liao. Displacements and stresses due to a vertical point load in an inhomogeneous transversely isotropic half-space. *Int. J. Rock. Mech. Min. Sci.*, 40, 667–685, 2003.
- [32] T. Kobayashi, F. Sasaki. Evaluation of Green’s-function on semi-infinite elastic medium. KICT Report, No. 86, Kajima Research Institute, Kajima Corporation, 1991.
- [33] G.R. Franssens. Calculation of the elastodynamic Green’s function in layered media by means of a modified propagator matrix method. *Geophys. J. R. Astro. Soc.*, 75, 669-691, 1983.
- [34] R. Cairo, E. Conte, G. Dente. Analysis of pile groups under vertical harmonic vibration. *Comput. Geotech.*, 32, 545-554, 2005.
- [35] E. Kausel. Generalized stiffness matrix method for layered soils. *Soil Dyn. Earthquake Eng.*, 115, 663–672, 2018.
- [36] H.M. Zhang, X.F. Chen, S. Chang. An Efficient Numerical Method for Computing Synthetic Seismograms for a Layered Half-space with Sources and Receivers at Close or Same Depths. *Pure Appl. Geophys.*, 160, 467-486, 2003.
- [37] A. Shaukath, R. Othman, A. Chamekh. Computation of harmonic green’s-functions of a homogeneous soil using an axisymmetric finite element method. *Int. J. Mech. Eng. Technol.*, 5, 169-182, 2014
- [38] A. Ammar, A. Zghal, F. Morel, F. Chinesta. On the space-time separated representation of integral linear viscoelastic models. *Comptes Rendus Mécanique*, 343(4), 247–263, 2015.
- [39] S. Metoui, E. Prulière, A. Ammar, F. Dau, I. Iordanoff. The proper generalized decomposition for the simulation of delamination using cohesive zone model. *Int. J. Num. Meth. Eng.*, 99(13), 1000-1022, 2014.
- [40] A. Dumon, C. Allery, A. Ammar. Proper Generalized Decomposition method for incompressible Navier-Stokes equations with a spectral discretization. *Appl. Math. Comput.*, 219, 8145-8162, 2013.
- [41] L. Boucinha, A. Gravouil, A. Ammar. Space-time proper generalized decompositions for the resolution of transient elastodynamic models. *Compt. Meth. Appl. Mech. Eng.*, 255, 67-88, 2013.
- [42] A. Ammar, E. Cueto, F. Chinesta. Non-incremental proper generalized decomposition solution of parametric uncoupled models defined in evolving domains. *Int. J. Num. Meth. Eng.*, 93, 887-904, 2013.
- [43] R. Ibáñez, A. Ammar, E. Cueto, A. Huerta, J.-L. Duval, F. Chinesta. Multiscale proper generalized decomposition based on the partition of unity. *Int. J. Num. Meth. Eng.*, 120, 727-747, 2019.

- [44] M. Vitse, D. Néron, P.A. Boucard. Dealing with a nonlinear material behavior and its variability through PGD models: Application to reinforced concrete structures. *Finite Elements in Analysis and Design*, 153, 22-37, 2019.
- [45] F. Louf, L. Champaney. Fast validation of stochastic structural models using a PGD reduction scheme. *Finite Elements in Analysis and Design*, 70-71, 44-56, 2013.
- [46] Barbarulo A. On a PGD model order reduction technique for mid-frequency acoustic. PhD Thesis, LMT-Cachan, 2012.
- [47] Barbarulo A., Ladeveze P., Riou H., Kovalevsky L. Proper Generalized Decomposition applied to linear acoustic: A new tool for broad band calculation. *Journal of Sound and Vibration*, 333, 2422-2431, 2014.
- [48] Germoso C., Aguado J. V., Fraile A., Alarcon E., Chinesta F. Efficient PGD-based dynamic calculation of non-linear soil behavior. *Comptes Rendus Mécanique*, 344, 24-41, 2016.
- [49] Haris M. M., Borzacchiello D., Aguado J. V., Chinesta F. Advanced parametric space-frequency separated representations in structural dynamics: A harmonic-modal hybrid approach. *Comptes Rendus Mecanique*, 346, 590-602, 2018.
- [50] Aguado J. V., Huerta A., Chinesta F., Cueto E. Real-time monitoring of thermal processes by reduced-order modeling. *International Journal for Numerical Methods in Engineering*, 102, 991-1017, 2015.
- [51] A. Ammar, F. Chinesta, E. Cueto, M. Doblaré. Proper generalized decomposition of time-multiscale models. *Int. J. Num. Meth. Eng.*, 90/5 : 569-596, 2012.
- [52] F. Chinesta, A. Ammar, A. Leygue, R. Keunings. An overview of the proper generalized decomposition with applications in computational rheology, *Journal of Non-Newtonian Fluid Mechanics*, 166/11 : 578-592, 2011.
- [53] F. Chinesta, A. Ammar, E. Cueto. Recent Advances in the Use of the Proper Generalized Decomposition for Solving Multidimensional Models. *Archives of Computational Methods in Engineering*, 17/4 : 327-350, 2010.
- [54] A. Ammar, F. Chinesta, A. Falco. On the Convergence of a Greedy Rank-One Update Algorithm for a Class of Linear Systems. *Archives of Computational Methods in Engineering*. 17/4 : 473-486, 2010.
- [55] A. Ammar, F. Chinesta, P. Diez, A. Huerta. An Error Estimator for Separated Representations of Highly Multidimensional Models. *Compt. Meth. Appl. Mech. Eng.*, 199 : 1872-1880, 2010.

- [56] F. Chinesta, A. Ammar, E. Cueto. Proper Generalized Decomposition of Multiscale Models. *Int. J. Num. Meth. Eng.*, 83 : 1114-1132, 2010.
- [57] A. Ammar. The Proper Generalized Decomposition: A Powerful Tool for Model Reduction. *International Journal of Material Forming*, 3 : 89-102, 2010.
- [58] M. S. Aghighi, A. Ammar, C. Metivier, F. Chinesta. Parametric solution of the Rayleigh-Benard convection model by using the PGD Application to nanofluids. *International journal of numerical methods for heat & fluid flow*, 25(6), 1252–1281, 2015.
- [59] A. Ammar, M. Normandin, F. Chinesta. Solving parametric complex fluids models in rheometric flows. *Journal of Non-Newtonian Fluid Mechanics*. 165 : 1588-1601, 2010.
- [60] A. Ammar, A. Huerta, F. Chinesta, E. Cueto, A. Leygue. Parametric solutions involving geometry: A step towards efficient shape optimization. *Compt. Meth. Appl. Mech. Eng.*, 268 : 178-193, 2014.

## A General framework of tensor product resolution

Let  $\Omega$  be a multidimensional domain involving  $N$  coordinates  $(x_1, x_2, \dots, x_N)$  (where each coordinate  $x_j$  is not necessarily one dimensional). Let consider a weak form of a linear problem given by :

$$a(\Psi(x_1, x_2, \dots, x_N), \Psi^*(x_1, x_2, \dots, x_N)) = b(\Psi^*(x_1, x_2, \dots, x_N)), \quad (96)$$

where we are looking to an approximated solution that writes in the continuous form as:

$$\Psi(x_1, x_2, \dots, x_N) = \sum_{j=1}^{n_F} \alpha^j F_1^j(x_1) F_2^j(x_2) \dots F_N^j(x_N). \quad (97)$$

The separated representation is built-up from a projection-enrichment iteration scheme. To this goal, we need to write the continuous expression in a discrete form using the nodal values of each function. This discrete form is given by:

$$\Psi = \sum_{j=1}^{n_F} \alpha^j F_1^j \otimes F_2^j \otimes \dots \otimes F_N^j. \quad (98)$$

Moreover, it is important to transform the weak form into a discrete form written as:

$$\Psi^{*T} \mathbf{A} \Psi = \Psi^{*T} \mathbf{B}, \quad (99)$$

where

$$\mathbf{A} = \sum_{j=1}^{n_F} A_1^j \otimes A_2^j \otimes \dots \otimes A_N^j, \quad (100)$$

and

$$\mathbf{B} = \sum_{j=1}^{n_F} B_1^j \otimes B_2^j \otimes \dots \otimes B_N^j, \quad (101)$$

The projection stage consists on finding the best set of  $\alpha^j$  coefficients. The associated test function is given by

$$\Psi^* = \sum_{j=1}^{n_F} \alpha^{*j} F_1^j \otimes F_2^j \otimes \dots \otimes F_N^j. \quad (102)$$

Substituting Eqs. (98), (100), (101) and (102) into Eq. (99) yields:

$$\sum_{i=1}^{n_F} \sum_{j=1}^{n_F} \alpha^{*i} H^{ij} \alpha^j = \sum_{i=1}^{n_F} \alpha^{*i} J^i, \quad (103)$$

where

$$H^{ij} = \sum_{k=1}^{n_A} \left( F_1^{iT} A_1^k F_1^j \right) \left( F_2^{iT} A_2^k F_2^j \right) \dots \left( F_N^{iT} A_N^k F_N^j \right), \quad (104)$$

and

$$J^i = \sum_{k=1}^{n_B} \left( F_1^{iT} B_1^k \right) \left( F_2^{iT} B_2^k \right) \dots \left( F_N^{iT} B_N^k \right). \quad (105)$$

The enrichment stage includes new candidates for enriching the reduced separated approximation basis such as:

$$\Psi = \underbrace{\sum_{j=1}^{n_F} \alpha^j F_1^j \otimes F_2^j \otimes \dots \otimes F_N^j}_{\Psi_F} + \underbrace{R_1^j \otimes R_2^j \otimes \dots \otimes R_N^j}_{\Psi_R}. \quad (106)$$

Within a fixed-point alternating direction algorithm, we look at each iteration for the computation of a single discrete function  $\underline{R}_j$  assuming all the others known. Thus, when we are looking for  $\underline{R}_j$  the test function writes:

$$\Psi^* = R_1 \otimes R_2 \otimes \dots \otimes R_{j-1} \otimes R_j^* \otimes R_{j+1} \otimes \dots \otimes R_N, \quad (107)$$

The different terms of the discrete weak form read:

$$\Psi^* \mathbf{A} \Psi_R = \sum_{k=1}^{n_A} \left( R_j^{*T} A_j^k R_j \prod_{\substack{h=1 \\ h \neq j}}^N R_h^T A_h^k R_h \right) = R_j^{*T} \mathbf{K} R_j \quad (108)$$

$$\Psi^* \mathbf{A} \Psi_F = \sum_{i=1}^{n_F} \sum_{k=1}^{n_A} \left( \alpha^i R_j^{*T} A_j^k F_j^i \prod_{\substack{h=1 \\ h \neq j}}^N R_h^T A_h^k F_h^i \right) = R_j^{*T} V, \quad (109)$$

and

$$\Psi^* \mathbf{B} = \sum_{k=1}^{n_B} \left( R_j^{*T} B_j^k \prod_{\substack{h=1 \\ h \neq j}}^N R_h^T B_h^k \right) = R_j^{*T} V' \quad (110)$$

In the framework of a fixed-point strategy we are looking, at each iteration, for the solution of the linear system:

$$\mathbf{K} R_j + V = V'. \quad (111)$$

We assume that the global convergence is attained when the error

$$\varepsilon = \|\mathbf{A} \Psi - \mathbf{B}\|_2. \quad (112)$$

becomes small enough. In terms of minimization, the previous variational formulation is equivalent to the minimization of the next functional

$$J(T) = (T - \mathbf{A}^{-1} \mathbf{B})^T \mathbf{A} (T - \mathbf{A}^{-1} \mathbf{B}) = \|T - \mathbf{A}^{-1} \mathbf{B}\|_{\mathbf{A}} \quad (113)$$